1 Kinetics of the LOV domain of ZEITLUPE determine its

circadian function in Arabidopsis†

2

3 4	Ashutosh Pudasaini ^a , Jae Sung Shim ^b , Young Hun Song ^{b,c} , Hua Shi ^d , Takatoshi Kiba ^e David E. Somers ^d , Takato Imaizumi ^b and Brian D. Zoltowski ^a *
5	^a Department of Chemistry, Southern Methodist University, Dallas, TX 75275, USA
6	Center for Drug Discovery, Design and Delivery, Southern Methodist University
7	^b Department of Biology, University of Washington, Seattle, WA, 98195-1800, USA
8	^c Department of Life Sciences, Ajou University, Suwon, 443-749, Korea
9	^d Department of Molecular Genetics, Ohio State University, Columbus, OH, 43210 USA
10	^e RIKEN Center for Sustainable Resource Science, Suehiro 1-7-22, Tsurumi, Yokohama, 230-
11	0045, Japan
12	* corresponding author:
13 14 15 16 17 18	Brian D. Zoltowski Assistant Professor, Department of Chemistry, Southern Methodist University Dallas, TX 75275-0314 t. 214-768-2640 f. 214-768-4089 e. bzoltowski@smu.edu
19	†Work was funded by the National Institutes of Health, Rural Development Administration, and
20	the Herman Frasch Foundation (R15GM109282 and 739-HF12 to B.D.Z., R01GM079712 to T.I.
21	SSAC, PJ011175 to Y.H.S and T.I., and R01GM093285 to D.E.S.)
22 23 24 25 26	

Abstract

A LOV (Light, Oxygen, or Voltage) domain containing blue-light photoreceptor ZEITLUPE (ZTL) directs circadian timing by degrading clock proteins in plants. Functions hinge upon allosteric differences coupled to the ZTL photocycle; however, structural and kinetic information was unavailable. Herein, we tune the ZTL photocycle over two orders of magnitude. These variants reveal that ZTL complexes with targets independent of light, but dictates enhanced protein degradation in the dark. *In vivo* experiments definitively show photocycle kinetics dictate the rate of clock component degradation, thereby impacting circadian period. Structural studies demonstrate that photocycle dependent activation of ZTL depends on an unusual dark-state conformation of ZTL. Crystal structures of ZTL LOV domain confirm delineation of structural and kinetic mechanisms and identify an evolutionarily selected allosteric hinge differentiating modes of PAS/LOV signal transduction. The combined biochemical, genetic and structural studies provide new mechanisms indicating how PAS/LOV proteins integrate environmental variables in complex networks.

Introduction

54

55

56

57

58

59

60

61

62

63

64

65

66

67

68

69

70

71

72

73

74

75

76

77

78

79

Organisms have developed signaling networks to measure and respond to daily (circadian) and seasonal (photoperiodic) alteration in environmental variables. Key to these circadian and photoperiodic responses is measurement of day length through complicated feedback loops involving sensory proteins. These sensory proteins involve members of the Period-ARNT-Singleminded and its Light, Oxygen, or Voltage (PAS/LOV respectively) subclass that couple photic-input to metabolic and stress pathways (1-3). Currently, how these signaling components are integrated is poorly understood due to a difficulty in decoupling photochemistry from allosteric protein changes and signal transduction. In plants and fungal species, LOV domain containing proteins act at signaling nodes to integrate sensory responses into circadian. reproductive and stress pathways (1, 4-6). Central to their function are two key elements of the PAS family: 1) The ability to sense and respond to diverse environmental stimuli, and 2) The presence of multiple interaction surfaces that engage targets in a selective manner (Figure 1. Figure 1-figure supplement 1). The ability to trigger these elements with light has positioned LOV proteins as an allosteric model and enabled the development of LOV optogenetic tools (7). However, limited understanding of how chemistry is linked to allostery and downstream signaling hampers our understanding of these systems.

Our current understanding of LOV signaling has benefited from detailed structural studies that revealed amino acid sites that tune LOV allostery without affecting LOV photocycle kinetics (6, 8-10). A consensus mechanism is summarized. LOV domains are typified by blue-light induced formation of a C4a adduct between a conserved Cys residue and a bound flavin (FAD, FMN or riboflavin) cofactor (Figure 1-figure supplement 1D) (11). C4a adduct formation then drives rotation of a conserved Gln residue to initiate conformational changes within N- or C-terminal extensions (Ncap/Ccap) to the LOV core (11). These N/Ccap elements in turn regulate activity of effector domains or recruit proteins to Ncap, Ccap or β -sheet surfaces (Figure 1-figure supplement 1A,C,E). Upon incubation in the dark, or in the presence of UV-A

light, the signaling adduct state spontaneously decays on a timescale of seconds to days (11-13). In this manner, LOV proteins dictate transiently stable signaling states capable of switching between a distinct on and off state depending on lighting conditions (6, 14-16). These photoswitchable functions have made LOV proteins targets for optogenetic devices; however, currently we have limited understanding of the role of LOV photocycle kinetics for *in vivo* function. Genetic and photochemical studies of plant circadian and photoperiodic timing indicate *Arabidopsis* may function as a model organism for delineating the roles of photochemistry and allostery in LOV function.

In *Arabidopsis thaliana*, three LOV domain containing proteins ZTL, FLAVIN-BINDING, KELCH REPEAT, F-BOX 1 (FKF1), and LOV KELCH PROTEIN 2 (LKP2) act in circadian timing and seasonal flowering (17). Among them, the genetic functions of ZTL and FKF1 are highly characterized. Recent research indicates that their divergent roles in the circadian clock and photoperiodic flowering may enable interrogation of how chemistry regulates PAS/LOV protein function to select for signaling pathways (Figure 1-figure supplement 1B) (18). These proteins retain analogous elements, where an N-terminal LOV domain regulates activity of a C-terminal E3 ubiquitin ligase to target clock proteins for degradation in a time dependent manner (17, 19). In addition, the LOV scaffold engages multiple proteins in a selective manner to regulate clock function (18). Despite conservation of domain elements, ZTL and FKF1 differ in their subcellular localization, degradation targets, and fundamental chemistry, thereby differentiating ZTL and FKF1 in circadian and photoperiodic timing (18).

Central to their function are key differences in photocycle kinetics. In FKF1, day-specific expression and a long-lived light-state species (τ =62 hours) enable light-specific functions (4, 7). In FKF1, photon absorption facilitates complex formation with GIGANTEA (GI) through its LOV domain (LOV-GI) to mediate degradation of CYCLING DOF FACTOR 1 (CDF1) and stabilization of CONSTANS (CO) (20-22). Here, selection of degradation or stabilization appears to center on the domain involved in target recruitment, where the Kelch repeat domain

(CDF1) specifies degradation and the LOV domain (CO) specifies stabilization (18, 23). Importantly, both functions require both light and GI.

106

107

108

109

110

111

112

113

114

115

116

117

118

119

120

121

122

123

124

125

126

127

128

129

130

131

In contrast, constitutive mRNA levels and a fast photocycle for ZTL (τ =1.4 hours) suggest possible day (light) and evening (dark) functions (13). Light-state ZTL has two primary functions, formation of a LOV-GI complex to allow protein accumulation during the day via enhanced ZTL/GI stability (24, 25), and ZTL/GI-dependent destabilization of CO in the morning (23). The latter results in antagonistic roles of ZTL and FKF1 in the photoperiodic response. and may contribute to a late-flowering phenotype in some ztl mutants (26). Throughout the night, ZTL mediates rapid degradation of the clock components, TIMING OF CAB EXPRESSION 1 (TOC1) and PSEUDO RESPONSE REGULATOR 5 (PRR5) (Figure 1-figure supplement 2) (27-29). TOC1 protein levels contribute to the control of period length of the circadian clock (18). Impaired degradation of TOC1 by ZTL mutants lead to accumulation of TOC1 and PRR5 protein and a long-period phenotype consistent with strains harboring additional copies of TOC1 (30). Interestingly, TOC1 degradation appears to be in competition with GI, occurs with an approximately 2-hour delay following dusk, and is enhanced in the dark (18, 19, 23, 25). Current models explain such behavior in TOC1/PRR5 turnover by imparting a differential function between day and night conditions (30, 31), where TOC1/PRR5 are targeted for degradation by ZTL regardless of lighting conditions, but degradation activity is enhanced in the dark. How this is achieved at the molecular and chemical level is not well understood.

Herein, we present a comprehensive study of ZTL signaling to develop a broad understanding of blue-light regulation of circadian and photoperiodic timing and to understand the evolutionary basis for divergent functions of ZTL and FKF1. Therein, we tackle two outstanding questions in the PAS/LOV field; 1) What purpose, if any, does the LOV photocycle lifetime play in biological function? Previous research proposed divergent roles for ZTL and FKF1 in the measurement of light intensity and day length (13), however no experimental validation of such a model has been available. Further, with the exception of a fungal system

(32), the role of LOV lifetimes in biology remains elusive. 2) How do PAS/LOV proteins signal to multiple interaction surfaces to allow signal integration? Based on structural studies of ZTL we have developed protein variants that decouple photocycle lifetimes from signal transduction. In this manner, we show a definitive role of LOV lifetime in circadian timing. Further, we provide an allosteric model of LOV signal transduction enabling selection of diverse protein:protein interactions.

Results

Examination of mathematical models of circadian function reveals that ZTL photocycle kinetics may impart phase specific degradation of TOC1 and PRR5 (30, 31). Namely by replacing indistinct day and night conditions by a difference in activity between light and dark-state ZTL, where the light-state inhibits ZTL activity in regards to degradation. In this manner, dark-state reversion activates ZTL during evening. Incorporating ZTL photochemistry into existing models of PRR5 results in equation 1 (see mathematical model generation in methods), where c_{PRR5} is the concentration of PRR5 protein, k_1 and k_2 the light and dark-state degradation constants and k_3 the rate of adduct decay for ZTL. An analogous equation, with equivalent k_3 dependence, can be derived for TOC1 (eq S12), however, the expression pattern of TOC1 and complex regulation of TOC1 mRNA complicates analysis of TOC1 levels during the circadian cycle. For these reasons, we use the simpler PRR5 degradation data to mathematically test our model and use a qualitative analysis for examining effects of k_3 on TOC1 (see below).

$$\frac{dc_{PRR5}}{dt} = -\{(k_1 - k_2)e^{-k_3t} + k_2\}c_{PRR5}$$
 [1]

Examination of equation 1 provides distinct predictions on the effect of the ZTL adduct decay rate constant (k_3) on PRR5 and TOC1 levels. If rate-altering variants only affect photocycle kinetics, k_3 would dictate delays in PRR5/TOC1 degradation (Figure 1). Under these conditions a long photocycle would lead to increasing delays in PRR5 and TOC1 degradation leading to

progressively longer circadian periods. Unfortunately, testing such predictions is complicated by difficulties in manipulating photochemical kinetics without altering allosteric regulation of ZTL function.

To delineate these aspects we focused on three residues in close proximity to the flavin active site that differ between ZTL and FKF1. These are G46 (Ser in FKF1) that lies adjacent to the active site Q154 implicated in Gln-flip signal transduction mechanisms (11), V48 (Ile in FKF1) that sterically interacts with C82 (33), and G80 that lies in a GXNCRFLQ motif (X80=G for ZTL, X=R for FKF1) (Figure 1-figure supplement 1E). The V48 position is known to alter LOV photocycle kinetics by V/I/T substitutions (33-36). This site has been exploited in optogenetic tools to tune signal duration under the presumption that it does not affect allosteric regulation of protein function (37). In contrast, to the best of our knowledge, the G80 position has not been exploited for tuning LOV kinetics. This likely is due to *Arabidopsis ZTL* being unusual amongst LOV proteins in containing a Gly residue at this position. As a consequence of G80, ZTL expresses poorly in *E. coli* and is largely confined to inclusion bodies (see methods). Since, G80 is unique to *Arabidopsis ZTL*, and R/Q/K substitutions are permitted in other ZEITLUPE and LOV proteins (see discussion), it is unlikely to affect allostery and may function as a site to uniquely affect photocycle kinetics.

Consistent with our predictions, kinetics of V48I and G80R differentiate ZTL and FKF1 type chemistry. Specifically, variants extend the ZTL lifetime from 1.4 hours (WT) to 6.6 (G80R) or 10.7 (V48I) hours (Figure 1-figure supplement 3 and Table 1). Double variants G46S:G80R and V48I:G80R function cooperatively to extend the ZTL photocycle to 21 hours or >65 hours respectively, very similar to WT FKF1 (62.5 hours) (13) (Figure 1-figure supplement 3 and Table 1). In addition, the difference in values for k₃ in these variants are sufficient to elicit theoretical differences in PRR5/TOC1 degradation rates (Figure 1B). To verify that rate-altering variants do not also perturb allosteric regulation of ZTL function it is essential to obtain crystal structures of ZTL variants and to map an allosteric trajectory that couples C4a adduct formation to

regulation of ZTL function. Towards these aims we solved 2.5 Å, 2.6 Å, and 2.1 Å crystal structures of dark-state WT ZTL, G80R and V48I:G80R (residues 29-165) respectively (see Table 2). In addition, the long-lived V48I:G80R variant enabled direct crystallization (2.3 Å) of the light-state adduct allowing for interrogation of signal transduction pathways.

ZTL structures reveal an unusual mechanism of signal transduction in LOV proteins. All ZTL variants form solution dimers, crystallize in the same space group (P3121) and demonstrate topologically equivalent structures consistent with PAS/LOV proteins (Figure 2, Figure 2-figure supplement 1,2). These structures reveal functional differences from all known LOV structures that differentiate the effects of V48I and G80R on ZTL signaling mechanisms. Namely, G80R structures are analogous to WT in all manners. The primary difference is the formation of a π -cation interaction that stabilizes the D α /E α linkage and C82 that is necessary for C4a adduct formation (Figure 2B). Increased rigidity of C82 imposed by the π -cation interaction is consistent with having an effect only on photocycle kinetics. In contrast, examination of V48I containing structures reveals distinct differences that identify allosteric signal transduction mechanisms to the N/Ccap. These mechanisms identify V48I as a residue that disrupts allosteric regulation of ZTL function. Below, we provide detailed analysis of ZTL in dark and light states to highlight these functional differences. We focus on two reported aspects of ZTL group function, LOV:LOV mediated homodimerization and allosteric regulation of Ncap and Ccap elements.

LOV dimerization. Previous solution studies of ZTL group proteins suggest they function as obligate dimers (38, 39), however ZTL group dimers have not been observed *in vivo* and their function is unknown (40). Consistent with solution studies, the crystallographic lattice is defined by two sets of anti-parallel dimers formed by extensive contacts along the β-scaffold. We term

these interfaces the "compact" and "elongated" dimers based on a 2 Å translation that is coupled to the degree of order present within the Ncap (Figure 2). In the compact dimer, clear density for Ncap residues (31-43) is observed in one molecule that contacts the helical interface of the adjacent monomer (Figure 2C,D). In contrast, the elongated dimer contains no density for Ncap residues (Figure 2E,F). A stabilizing element in both dimers is a hydrophobic core composed of a tetrad of lle residues (I151 and I153).

Additional contacts along the helical interface define a possible secondary dimer. The helical dimer is parallel in orientation and involves contacts between the E-F helices and associated loop. Specifically, R95 forms a salt bridge with the phosphate moiety of FMN in the neighboring molecule (Figure 2—figure supplement 2). However, based on two lines of evidence, we conclude that the β -scaffold interface represents the solution ZTL and FKF1 homodimers. First, FKF1 lacking the entire E-F loop and ZTL variants that disrupt R95 contacts remain dimeric (Figure 2—figure supplement 2) (39). Second, I151R (and I160R in FKF1) variants abolish dimer formation *in vitro* (Figure 2A and Figure 2—figure supplement 1). Thus, ZTL and FKF1 solution dimers are formed by equivalent anti-parallel contacts along the β -scaffold, similar to other PAS/LOV proteins (41).

N-terminal CGF motif defines a locus of signal transduction that differentiates ZTL from known LOV signaling mechanisms. Given the unknown role of ZTL dimers *in vivo* and the known role of Ncap and Ccap elements in LOV allostery, we turned our attention to the structural differences between the different dimers. Close examination of residues linking the Ncap and Ccap to the active site FMN identifies distinguishing interactions that may be involved in signal transduction. The loss of Ncap density in the elongated dimer directly follows a CGF motif (C45-G46-F47-(V48)) that links the Ncap, FMN binding pocket and the V48 position (Figure 3). An analogous hinge involving a Cys residue is known to mediate signal transduction

in fungal LOV proteins, where the hinge directs both a conformational change and integration of oxidative and osmotic stress (1, 6, 33, 36, 42, 43). Further, the CGF motif differentiates ZTL and FKF1, where FKF1 contains the G46S and V48I (equivalent) mutations, thereby highlighting the region as a possible factor regulating the divergent functions of these closely related proteins.

In ZTL, signal transduction diverges from known LOV signaling mechanisms (Figure 3 and 4). In contrast to other LOV proteins, where a conserved Gln (Q154) acts as a molecular bridge linking the FMN to a residue in A β , the dark-state structure of ZTL contains a heterogeneous orientation of the active site Q154 (Figure 3 and Figure 3—figure supplement 1) (6, 14, 44). The altered orientation is coupled to contacts in the Ncap, Ccap and helical interface. Given that all three sites have been implicated in PAS/LOV signaling (8, 41, 43, 45), we examine each interaction below. We define them as the A β -Ncap hinge, I β -Ccap hinge and C α (helical interface) to specify structural elements that may be involved in signal transduction.

In ZTL, Q154 does not adopt a specific orientation as observed in all other LOV structures, rather it varies in all four molecules in the asymmetric unit of both WT-ZTL and G80R (Figure 3A and Figure 3—figure supplement 1). The altered conformations contact the A β -Ncap hinge through G46 in the CGF motif (Ncap; Figure 3B). Here, Q154 abuts (3.4 Å) the C α carbon of G46 (Ser in FKF1). The lack of a side chain at G46 permits favorable interactions for Q154 at the flavin O4 position and allows insertion of F156 into the flavin active site. In this manner an unusual orientation of Q154 links the I β -Ccap hinge and helical interface through a QFF motif (Q154-F155-F156). In most LOV proteins, the equivalent residue to F156 is hydrophilic and adopts a solvent exposed position (Figure 3). The resulting cavity occupied by F156 is filled by a Met or Leu residue (V69 in ZTL) from C α (Figure 3B,D). In ZTL, the altered orientation of Q154 clashes with typical orientations of C α . Steric clashes lead to movement of conserved F66 and rotation of V69 away from Q154 and the FMN binding pocket.

The combined interactions stemming from Q154 positions it ideally to have concerted conformational changes within Ncap and Ccap elements. Although, the Gln locus has been cited as the primary source of signaling in LOV proteins (6, 14, 46), the lack of interactions near N5 and A β is atypical. Thus, it is likely that ZTL does not involve an H-bonding switch in signal transduction and that canonical mechanisms of LOV signaling may not be universally conserved. Rather, we propose that steric interactions involving the flavin O4 position and G46 shift a dynamic equilibrium in the Q154 position to stabilize the ZTL protein in a light-state configuration. We posit that the heterogeneous orientation of Q154 destabilizes ZTL in the absence of covalently attached FMN, consistent with *in vitro* studies demonstrating a tendency to lose flavin rapidly. Upon light activation, ZTL is stabilized by covalent attachment of FMN (through C82) and results in movement of Q154 that necessitates rearrangement of the CGF, QFF and C α sites to elicit signal transduction.

Dark and light state structures of V48I:G80R confirm concerted movement of Q154 that is linked to conformational changes in V/I48. The Q154 conformation is not heterogeneous in V48I:G80R, rather, the lle side chain sterically directs Q154 to an exposed conformation near O4 that has not been observed in other LOV proteins. Comparing the dark-state to V48I:G80R grown in the light, confirms density for the C4A adduct and confirms direct crystallization of the light-state (Figure 4). Difference density maps of the light-state molecule indicate that adduct formation is coupled to rotation of Q154 to a buried position (Figure 4C). Unexpectedly, rotation of Q154 requires concerted movement of I48 that reorients the Ncap. Thus, the presence of G46 selects for a heterogeneous conformation of Q154 and V48I biases the heterogeneous Q154 towards the exposed conformation in the dark. In the light, V48I disrupts rotation of Q154 to the buried conformation, thereby leading to a predominantly exposed conformation regardless of lighting conditions. Thus, unexpectedly, V48I is both an allosteric variant and alters photocycle kinetics. In particular, V48I retains an ability to form the covalent C4a adduct,

which is more stable than WT (V48I k_3 =0.094 hr⁻¹; WT k_3 =0.71 hr⁻¹). However, in V48I allosteric regulation of the Ncap through Q154 is disrupted leading to V48I selecting for a distinct exposed Q154 conformation despite adduct formation (Figure 4).

Based on our structural results we can refine our models on how ZTL rate altering variants will perturb ZTL function. G80R does not impact ZTL structure or allosteric regulation of Ncap or Ccap elements. In this manner, G80R acts as a photocycle variant only and allows direct testing of LOV photocycle kinetics on targeted degradation of PRR5 and TOC1 (see Eq. 1). In contrast, despite being photochemically active and stabilizing the C4a adduct, V48I blocks allosteric regulation of the Ncap through incomplete rotation of Q154 and selection of a distinct exposed conformation of Q154. Thus, we propose that V48I is an allosteric variant that mimics the degradation-active dark state. Combining our proposed mechanism with equation 1 above and existing literature on light-dark formation of ZTL:GI complexes we make the following testable hypotheses: 1) V48I should demonstrate weaker interactions with GI. 2) V48I should show constitutive activity regardless of lighting conditions in targeting PRR5 and TOC1 for degradation. Thus, PRR5 and TOC1 levels should be constitutively low in variants containing the V48I mutation.

V48I disrupts ZTL:GI interactions. We examined ZTL variants for their ability to form light and dark regulated complexes with GI and ARABIDOPSIS SKP1-LIKE 2 (ASK2) of the SCF complex. CoIP results confirm that G80R retains light regulated complex formation with GI comparable to WT. In contrast, Ncap variants G46S and V48I both alter light driven complex formation with GI (Figure 4—figure supplement 1). Whereas, V48I leads to dampened light-driven formation of the ZTL:GI complex, G46S enhances GI complex formation in both the dark-and light-states (Figure 4—figure supplement 1A). These results support our allosteric model of ZTL regulation and demonstrate that Ncap variants decouple allosteric regulation of signal transduction from photochemical formation of the C4a adduct. Further, the data implicates light-

driven conformational changes near the Ncap in dictating GI interactions. Specifically, where V48I mimics the weak GI interacting dark-state and G46S mimics the strong GI interacting light state. We note that the G46S results reported here diverge from the effects of the G46E mutation reported by Kim et al. (25), where G46E abolishes GI interactions due to apparent misfolding of the LOV domain. These results are informative on the nature of mutations at the G46 site, namely the long side chain present in a G46E variant leads to steric clashes and likely would force E46 into a hydrophobic pocket (see Figure 4—figure supplement 2). We contend such clashes leads to the destabilization of the LOV domain and abolition of GI interactions as reported previously for G46E (25). In contrast, the shorter sidechain in G46S, can be easily accommodated by a subtle rotation of the active site Q154 towards the proposed light-state buried conformation (modeled in Figure 4—figure supplement 2). Such results are consistent with enhanced GI interactions in G46S. Combined, the results implicate the G46/V48 locus in ZTL allostery and regulation.

In contrast to GI, where G46/V48 mutations affect function in a light/dark manner, all ZTL variants complex with ASK2 in a light-independent manner comparable to WT (Figure 4—figure supplement 1B). The protein:protein interaction data confirms G80R behaves as WT in known biochemical functions of ZTL and only differs in photocycle kinetics. In contrast, V48I acts as an allosteric variant mimicking the dark-state conformation. Based on these results and previously published *in vivo* studies showing enhanced degradation activity in the dark (19), we have tools to test the effect of photocycle kinetics (G80R) and Ncap allostery (G46S/V48I). In this manner, G80R variants isolate effects of photocycle kinetics allowing testing of predictions based on equation 1.

The decrease in GI affinity in the V48I variant could complicate *in vivo* phenotypes for these variants. Literature indicates ZTL stability is dictated by GI interactions (25). Thus, we could expect low ZTL levels in V48I variants. These low ZTL levels would act in opposition to any increased targeted degradation of PRR5/TOC1 and could mask allosteric phenotypes.

Based on our experimental conditions, we do not expect any complications to result. Prior studies indicate that ZTL and GI reciprocally stabilize each other (24, 25), but increased ZTL stability occurs in a circadian phase dependent manner (47). Light does enhance ZTL:GI affinity and reciprocal stability by three fold, but ZTL retains some stabilization during the subjective circadian day regardless of lighting conditions (25, 47). These previous findings suggest that in consideration of the ZTL:GI equilibrium, GI is limiting except during the subjective circadian day. During the day, GI levels rise sufficiently to shift the equilibrium to saturate the ZTL:GI complex regardless of lighting conditions. Given that our V48I variant retains light-state affinity comparable to WT dark-state protein, GI expression during the subjective day under LL conditions should rescue the decrease in affinity. Concomitant with ZTL-ox, reciprocal stabilization of ZTL/GI should lead to high ZTL levels and ZTL should no longer oscillate. Indeed, under our experimental conditions cycling of ZTL protein is lost and V48I variants show enhanced stability in vivo (Figure 5—figure supplement 1), thereby the role of GI in ZTL stability is masked under our conditions and our results likely reflect the effect of ZTL photochemistry (G80R) and allosteric activation of PRR5/TOC1 degradation (V48I) independent of the effects on GI binding.

Based on the data above we make the following predictions. In comparing G80R-ox to WT-ox under LD conditions, the fast decay of WT-ox will lead to higher populations of the active-dark state early in the evening. In contrast, slower adduct decay in G80R will lead to prolonged population of the less active light-state and delays in ZTL degradation activity. As a result, we should observe an enhanced delay in PRR5/TOC1 degradation in G80R variants as shown in Figure 1 and Figure 5—figure supplement 2. For V48I and V48I:G80R, the allosteric effects should enhance degradation of PRR5 and TOC1 leading to constitutively low PRR5/TOC1 levels.

334

335

336

337

338

339

340

341

342

343

344

345

346

347

348

349

350

351

352

353

354

355

356

357

ZTL variants alter targeted degradation of clock components. To test our predictions, we constructed *Arabidopsis* transgenic ZTL overexpression lines (ZTL-ox) containing WT, V48I, G80R and V48I:G80R. G46S variants were excluded due to poor yields from *E. coli* that render solution or structural information intractable for the isolated G46S variant (see methods). These constructs were then examined for their effect on PRR5 and TOC1 degradation as well as circadian period and amplitude. All transgenic lines were selected based on similar *ZTL* transcript levels and ZTL protein levels were measured (Figure 5—figure supplement 1).

Consistent with our predictions, G80R-ox (#22) leads to delayed degradation of PRR5 and TOC1 under LL and LD (Figure 5). Specifically, despite being overexpressed (Figure 5—figure supplement 1A), G80R-ox variants demonstrate peak amplitudes of TOC1 consistent with WT (Figure 5A,B). Further, comparison of apparent rate constants for PRR5 degradation confirms a direct effect of ZTL photocycle kinetics on PRR5 degradation, where G80R #22 (0.34 hr⁻¹ LD, 0.14 hr⁻¹ LL) exhibits smaller rate constants compared to WT-ox (0.5 hr⁻¹ LD, 0.13 hr⁻¹ LL) under LD conditions where k₃ is most relevant (Table 3). These results are consistent with a more active dark-state ZTL. Thus, ZTL photocycle kinetics regulate degradation of TOC1/PRR5.

Examining V48I and V48I:G80R variants confirms a role of V48I in altering light-dark regulation of ZTL activity. Strains harboring V48I and V48I:G80R show constitutively low levels of PRR5 and TOC1, consistent with high degradation activity regardless of lighting conditions (Figure 5). Both variants show degradation rate constants for PRR5 of ~0.8-1 hr⁻¹ under LD conditions, similar to maximum rate constants (0.8 hr⁻¹) predicted from computation models of clock function (30, 31) (see methods and Table 3). V48I and V48I:G80R also exhibit high activity under LL conditions, demonstrating a partial loss of light-dark regulation (Figure 5 and Table 3). Combined, G80R confirms a direct role of LOV photocycle kinetics on ZTL activity and that V48I acts in an allosteric switch to enable light-state V48I (adduct formation) to mimic the more degradation active and less GI-binding competent dark-state.

ZTL variants alter circadian period. Given the effect of V48I, G80R and V48I:G80R on PRR5 and TOC1 degradation, these variants should have predictable effects on circadian period. Previous studies of ZTL-ox variants demonstrate a dose dependent effect of ZTL on circadian period, where high protein levels lead to short-period phenotypes progressing to arrhythmicity and ZTL-nulls having a long-period phenotype (26). Similarly, TOC1 overexpression strains have a long-period phenotype and TOC1-null strains have short periods (29, 48). Thus, we predict that despite overexpression the defect in degradation of TOC1 by G80R-ox should lead to WT periods. In contrast, low TOC1 levels in V48I and V48I:G80R should lead to arrhythmic phenotypes under expression levels comparable to WT-ox strains demonstrating normal periods.

Indeed examination of circadian periods in WT and mutant-ox strains confirms predicted effects of photocycle kinetics (G80R) and the signaling defect (V48I) on circadian period. All strains containing V48I lead to an arrhythmic phenotype consistent with heightened degradation activity in these variants (Figure 6 and Table 3). In contrast, G80R-ox strains harboring 3-times more ZTL protein than WT has a circadian period indistinguishable from WT and WT-ox (see Table 3; 35S:HA-ZTL (G80R) #22; 24 hours, compared to WT; 24 hours and 35S:HA-ZTL #17; 24 hours). Only when protein levels exceed 10-fold higher than WT-ox is the period shortened to 19 hours (35S:HA-ZTL (G80R) #23) (Figure 6 and Table 3). These results confirm that ZTL photocycle kinetics are coupled to selection of circadian period through PRR5/TOC1 degradation.

Discussion

Insight into ZTL function in Arabidopsis.

In *Arabidopsis thaliana*, ZTL and FKF1 diverge in their diurnal pattern of transcription and function. Whereas, FKF1 function and transcription is specific to the day, ZTL demonstrates constitutive transcription and distinct functions during the day and night (23). These distinct functions allow ZTL to impact photoperiodic flowering through morning specific

411

412

413

414

415

416

417

418

419

420

421

422

423

424

425

426

427

428

429

430

431

432

433

434

435

and GI-dependent destabilization of CO, and circadian function through night specific degradation of TOC1 and PRR5 (19, 23, 27). These results suggest that both light (CO destabilization/GI interaction) and dark (TOC1/PRR5 degradation) activate ZTL for function. Such observations seem paradoxical; however, examination of our structural and kinetic results indicates ZTL may use a divergent allosteric mechanism to enable dual light/dark functions.

The ability of LOV domains to function as photoswitchable proteins is predicated on LOV proteins specifying a distinct light- and dark-state configuration. In all dark and light-state LOV structures currently in the protein data bank, the active site Gln (Q154 in ZTL) adopts a distinct buried conformation in the dark, with the NH moiety of the Gln side chain near flavin-N5 (6, 14). Existing light-state structures indicate that C4a adduct formation and N5 protonation induces rotation of the Gln side chain to favor an H-bond between flavin-HN5 and the O moiety of the Gln side chain (49). In those structures, the Gln residue maintains the buried conformation and is only distinguished by the nature of H-bonds. In our ZTL structures this is not the case, rather dark-state structures have a heterogeneous orientation of Q154 that samples orientation near both the buried conformation and an exposed conformation (Figure 3—figure supplement 1). A heterogeneous conformation of the key signaling switch would suggest poor regulation of function under dark-state conditions. This is exactly what is observed in ZTL. ZTL retains fairly robust activity for GI interactions and TOC1/PRR5 degradation in both the light and dark, with light enhancing GI interactions and repressing TOC1/PRR5 degradation by 3-5 fold (25) and (Table 3). As such, GI-dependent function in CO destabilization is likely not a light-regulated event, but rather is a combined result of constitutive transcription of ZTL, day-specific expression of GI and poor signal amplification following light-dark interconversion due to the heterogeneous orientation of Q154. Thus, the unusual Gln orientations appear to be evolutionarily selected to permit light- and dark-state functions of ZTL and to differentiate ZTL and FKF1.

Combining our dark- and light-state structures with in vivo data allows construction of a putative signaling mechanism differentiating ZTL from other LOV proteins. Examination of the ZTL structures identifies two key residues involved in regulating ZTL allostery. The heterogeneous conformation of Q154 is permitted by the lack of a sidechain in G46 (model in Figure 4—figure supplement 2). Introduction of V48I, directs Q154 to a single exposed conformation in the dark. Biasing the Q154 to the exposed conformation results in disrupted interactions with GI and high TOC1/PRR5 degradation, in vivo, consistent with selecting for a distinct dark-state conformation. Further, the light-state V48I:G80R molecule indicates partial Q154 rotation to a buried conformation that is impeded by V48I. This impediment does not allow robust sampling of the buried conformation under any lighting conditions and coincides with constitutively high TOC1/PRR5 degradation in V48I containing variants. Combined we propose a putative model of ZTL signaling (Figure 4). ZTL retains functionality in the light and dark due to a heterogeneous orientation of Q154 permitted by G46 and V48. Differences in functionality between dark/light result from subtle biases in the orientation of Q154 between buried and exposed conformations. Based on V48I:G80R structures and activity, we propose that biasing towards the exposed conformation as the dark-state configuration (enhanced PRR5/TOC1 degradation) and biasing towards the buried conformation as the light-state configuration (enhanced GI binding).

454

455

456

457

458

459

460

461

436

437

438

439

440

441

442

443

444

445

446

447

448

449

450

451

452

453

G46 and V48 are evolutionarily selected to differentiate ZTL and FKF1 in plants.

Based on our proposed mechanism distinguishing ZTL signal transduction from other LOV proteins, one would predict evolutionary selection of G46 and V48 in ZTL proteins to permit the heterogeneous orientation of Q154. Phylogeny of LOV sequences in planta demonstrates evolutionary selection of residues G46, V48 and F156 to differentiate ZTL-like, FKF1-like and phototropin-like (LOV2) proteins and putative signal transduction pathways (Figure 7 and Figure 7—figure supplement 1). Specifically, in monocots and dicots ZTL-like proteins conserve the

G46 that is necessary for selection of the exposed conformation of Q154. In FKF1 (monocots: A46 and dicots: S46), phototropins (N46) and all other structurally characterized LOV proteins, an H-bond or sterically directing residue occupies this position.

Residue selection at position 46 is coupled to V48. V48 is conserved in ZTL, but substitutions are permitted in FKF1, phototropins and fungal LOVs (Figure 7—figure supplement 1) (1, 6). The altered signaling mechanism in ZTL is supported by examination of LOV proteins in Brassica rapa. ZTL-like proteins in Brassica and AtLKP2 contain a Q154L substitution, resulting in an LXF consensus sequence at that locus. The presence of a Q154L substitution is unexpected, since these substitutions abrogate blue light signaling in other LOV proteins due to an inability to undergo the Gln-flip mechanism (6, 50, 51). In the proposed ZTL mechanism a Gln-flip is not necessitated and Q→L substitutions are permitted. In this manner, our understanding of a canonical model of LOV signal transduction is incomplete. We propose that evolutionary selections at G46 and V48 tune allostery to the Ncap through the Q154 orientation to differentiate modes of LOV signal transduction. Given the evolutionary selection of A/S residues and permission of V48 substitutions in FKF1, we propose that FKF1 functions in a manner analogous to other LOV proteins, where light activates the biological function (CO stabilization/CDF degradation) of the primarily nuclear FKF1 protein. In this manner, evolutionary selection at position 46 may dictate day functional (FKF1) and day/night functional (ZTL) differentiation, thereby implicating LOV photocycle kinetics as being imperative for proper signal transduction.

482

483

484

485

486

487

462

463

464

465

466

467

468

469

470

471

472

473

474

475

476

477

478

479

480

481

ZTL:TOC1/PRR5:GI circuit dictates circadian period through LOV kinetics.

Currently, delays in TOC1 and PRR5 degradation are explained using competition between GI and TOC1/PRR5 for the available ZTL pool (19, 25, 27, 28). In these models, GI expression during the day both stabilizes and sequesters ZTL. In the evening, GI pools decline leading to active free ZTL. In light of our data, the competition model must be incomplete. In

the competition model there should be no differences in the LL/LD characteristics in WT and G80R strains. In the competition model GI expression profiles should dictate delays and these would be unaffected by rate-altering ZTL variants. WT and G80R interact with GI to comparable levels, yet G80R demonstrates enhanced delays in PRR5 and TOC1 degradation (Figure 5D). These results are inconsistent with a competition model alone. In contrast, modeling PRR5 degradation using the time dependent conversion of ZTL-light to ZTL-dark can predict with reasonable certainty the extended delay in G80R and predicts distinct differences under LL conditions between the two proteins (Figure 5—figure supplement 2). In this manner, it is clear that ZTL photocycle kinetics are instrumental in dictating delays in PRR5/TOC1 turnover and circadian period.

Based on all these elements we propose that circadian period is regulated in a complex manner involving a ZTL:TOC1:GI circuit, whereby competitive inhibition and ZTL photocycle kinetics act in concert to dictate ZTL protein levels and ZTL activity in a circadian phase dependent manner. Adduct decay in ZTL then enhances degradation of PRR5 and TOC1, impacting circadian period through two methods: 1) Degradation of PRR5, helps diminish TOC1 levels through increased cytosolic retention and accessibility to ZTL (52) and 2) Degradation of cytosolic TOC1. Both factors require proper ZTL photocycle kinetics. Thus, LOV photocycle kinetics are instrumental in evolutionary selection for a 24-hour period.

Acknowledgments

This work is based on research conducted at the Cornell High Energy Synchrotron Source (CHESS). CHESS is supported by the NSF & NIH/NIGMS via NSF award DMN-0936384, and by NIGMS award GM-103485. We thank the Herman Frasch Foundation (739-HF12 to BDZ) the NIH (R15GM109282 to B.D.Z, R01GM079712 to T.I. and R01GM093285 to D.E.S.), Next-Generation BioGreen 21 Program (SSAC, PJ01117501 to Y.H.S. and PJ01117502 to T.I, Rural Development Administration, Republic of Korea) and NSF (MCB-1613643 to BDZ) for funding.

We thank Elaine Tobin for generously providing TOC1 antibody and Robert Green for experimental assistance.

Methods:

Model Generation

Examination of recent mathematical models of plant circadian clocks reveals a common method of incorporating light-dark dependent degradation of PRR5 and TOC1 by ZTL. In Pokhilko *et al.*, PRR5 and TOC1 levels are treated as follows (31):

$$\frac{dc_{p5}}{dt} = p_{10}c_{p5}^m - (m_{17} + m_{24}D) * c_{P5}$$
 [S1]

$$\frac{dc_{TOC1}}{dt} = p_4(c_{TOC1}^m + n_{16}) - (m_6 + m_7 D) * c_{TOC1} * (c_{ZTL} * p_5 + c_{ZG}) - m_8 c_{TOC1}$$
 [S2]

Where C_x represent protein concentrations, C_x^m , mRNA levels, p_x , n_x and m_x are parameters fit to data sets. ZG represents the ZTL:GI complex. D represents darkness, where D=1 at night and D=0 during the day. Both equations are constructed of similar elements, a protein synthesis term defined by mRNA levels and a degradation term defined by PRR5/TOC1 protein levels, and in the case of TOC1 the total ZTL protein pool. We note, that ZTL protein levels are not incorporated into existing models of PRR5 degradation (30, 31) suggesting that overexpression has a weak enough effect on the overall rate of PRR5 degradation that models lacking ZTL concentration can accurately predict degradation kinetics. Although biologically such an analysis is incomplete, for modeling purposes the accuracy of these prior models suggests this assumption is reasonably valid. Therefore, they normalize the ZTL concentration to 1 and it does not appear in the PRR5 degradation term. Further, in the fit parameters, p5=1, which allows simplification as shown in eq. S4, where c_{ZTL} now equals the total pool of ZTL protein regardless of whether free or in complex with GI.

For our purposes, ZTL rate altering variants should not perturb the transcription rates, therefore differences in PRR5/TOC1 degradation should be limited to the degradation terms. For PRR5 and TOC1 the degradation terms are as follows

$$\frac{dc_{p5}}{dt} = -(m_{17} + m_{24}D) * c_{p5}$$
 [S3]

$$\frac{dc_{TOC1}}{dt} = -(m_6 + m_7 D) * c_{TOC1} c_{ZTL} - m_8 c_{TOC1}$$
 [S4]
The above equations do not incorporate ZTL photochemistry, rather, the term m*D to enhance

The above equations do not incorporate ZTL photochemistry, rather, the term m*D to enhance the degradation rate constant under dark state conditions. In the dark, D=1 and the degradation rate constant (k_2) becomes ($m_{17}+m_{24}$) or (m_6+m_7) for PRR5 and TOC1 respectively. In the light, D=0 and the rate constants (k_1) reduce to m_{17} and m_6 . To add ZTL photochemistry to these equations we rewrite these degradation equations in terms of light and dark-state ZTL. We also note additional complications in the TOC1 equation. The term m_8*c_{TOC1} is a non-ZTL dependent degradation term, presumably accounting for nuclear degradation of TOC1. Because of the additional complexities in TOC1 expression and non-ZTL dependent degradation we do not model TOC1 degradation *in vivo*, we do however show below that the rate constant for LOV adduct decay, k_3 , will impact TOC1 in a manner analogous to PRR5.

553
$$\frac{dc_{p5}}{dt} = -(k_1 * c_{ZTL-L} + k_2 * c_{ZTL-D}) * c_{P5}$$
 [S5]

555
$$\frac{dc_{TOC1}}{dt} = -(k_1 * c_{ZTL-L} + k_2 * c_{ZTL-D}) * c_{TOC1} - m_8 * c_{TOC1}$$
 [S6]

Where k_1 , k_2 are the rate constant for degradation in the light and dark respectively. Similarly, c_{ZTL-L} and c_{ZTL-D} represent the light and dark-state levels of ZTL. We also normalize the total ZTL concentration to 1. Doing so allows calculation of c_{ZTL-L} and c_{ZTL-D} as a function of time during the dark-phase of LD cycles, by incorporating the rate constant for adduct decay, k_3 .

$$c_{ZTL-D} = 1 - c_{ZTL-L}$$
 [S7]

$$c_{ZTL-L}(t) = e^{-k_3 t}$$
 [S8]

It follows that:

$$\frac{dc_{p5}}{dt} = -[k_1 * c_{ZTL-L} + k_2 * (1 - c_{ZTL-L})] * c_{P5}$$
 [S9]

$$\frac{dc_{p5}}{dt} = -[(k_1 - k_2) * e^{-k_3 t} + k_2]c_{p5}$$
 [S10]

569 Similary:

570
$$\frac{dc_{TOC1}}{dt} = -[k_1 * c_{ZTL-L} + k_2 * (1 - c_{ZTL-L})] * c_{TOC1} - m_8 * c_{TOC1}$$
 [S11]

572
$$\frac{dc_{TOC1}}{dt} = -[(k_1 - k_2) * e^{-k_3 t} + k_2]c_{TOC1} - m_8 * c_{TOC1}$$
 [S12]

We note, that a compact model of clock function by De Caluwe *et al.* demonstrates that existing data can be adequately fit for both PRR5 and TOC1 levels using an analogous equation for both PRR5 and TOC1 (only the degradation term has been extracted) (30).

$$\frac{dc_{PT}}{dt} = -(k_D D + k_L L) * c_{PT}$$
 [S13]

Where, k_D , k_L are the light and dark degradation rate constants respectively, and L and D reference the lighting conditions, where L=1, D=0 during the day and L=0, D=1 during the evening. C_{PT} represents either the PRR5 or TOC1 level. Applying our method above to the De Caluwe *et al.* model (Eq. S13), results in an analogous expression as Eq. S10.

Thus, in terms of ZTL chemistry, PRR5 and TOC1 degradation should be dictated by k_3 . Using mutants that affect only k_3 , see table 1, one should be able to accurately model PRR5 decay rates *in vivo*. Again we note that the expression pattern of TOC1 and complex regulation of TOC1 mRNA complicates TOC1 levels during the circadian cycle. For these reasons, we use the simpler PRR5 degradation data to mathematically test our model above and use qualitative differences in degradation patterns to examine effects of k_3 on TOC1.

Parameter estimation for Figure 1B.

To predict how k_3 may affect delays in PRR5 degradation we required estimates of k_1 and k_2 . Examining Pokhilko *et al.* and De Caluwe *et al.* provides reasonable bounds for parameter estimation. First, PRR5 models suggest that PRR5 can be accurately modeled excluding differences in ZTL expression levels (30, 31), this is consistent with our data showing that WT, WT-ox and G80R-ox all have the same decay rate under LL conditions despite differences in protein levels. Second, in De Caluwe *et al.* the maximum degradation rate constant for PRR5 degradation was fit as 0.78 hr⁻¹. Similarly, in Pokhilko *et al.* a max value of 0.5 hr⁻¹ was obtained for PRR5 and a k_{max} of 0.8 hr⁻¹ for TOC1 by combining all degradation

terms. Given the similarity of these maximum values we chose a k_{max} for the dark-state of 0.8 hr⁻¹. The lowest fit rate constant in mathematical models is m_6 (0.2 hr⁻¹) for TOC1 degradation under light-state conditions. Thus, we used 0.2 hr⁻¹ as an estimate of PRR5/TOC1 degradation in the light.

Data was then simulated by numerically solving eq. S9 in matlab using the following parameters and plotted in Figure 1B.

```
602 k_1=0.2 \text{ hr}^{-1}
603 k_2=0.8 \text{ hr}^{-1}
```

- 604 k₃=0.7 hr⁻¹ (WT), 0.15 hr⁻¹ (G80R), 0.09 hr⁻¹ (V48I), 0.05 hr⁻¹ (G46S:G80R), 0.02 hr⁻¹ (V48I:G80R)
- 605 PRR5(0)=1

- Values for k₃ are derived from experimental values for the adduct decay time constant
- 608 (τ) present in table 1, where $k_3=1/\tau$.

Fitting model to experimental data.

To estimate the relative accuracy of our model depicted in Eq. S10, we extracted improved estimates of k_1 and k_2 from the experimental data shown in Fig. 5D.

Our structural data indicates that V48I mimics the dark-state regardless of lighting conditions, thus, V48I degradation kinetics under LD serves as a reasonable estimate for k_2 , the dark-state rate constant. We note, that our experimental value for V48I (0.8 hr⁻1) is identical, to the k_{max} values present in both Pokhilko *et al.* and De Caluwe *et al*, which should reference the more active dark-state value.

Under LL conditions we observe a rate constant for PRR5 degradation of 0.13-0.14 hr⁻¹ for WT, WT-ox and G80R. Under our lighting conditions (broad spectrum; 40-50 μ mol m⁻²s⁻¹), the light-state should be near saturated, and thus in the absence of allosteric effects should report the light-state degradation rate constant. We use 0.14 hr⁻¹ then as an estimate for k₁ the light-state rate constant.

We note the similarity of values between the three strains despite different expression levels. These results suggest that the models by Pokhilko *et al.* and De Caluwe *et al.*

demonstrating a weak dependence of PRR5 degradation on ZTL expression levels is reasonably valid under our conditions. Further, it provides a reasonable estimate for k_1 the light-state degradation term.

Thus, to test the accuracy of our model we numerically solved eq. S9 in matlab using:

- $k_1=0.14 \text{ hr}^{-1}$
- $k_2=0.8 \text{ hr}^{-1}$
- $k_3=0.7 \text{ hr}^{-1} \text{ (WT)}, 0.15 \text{ hr}^{-1} \text{ (G80R)}$
- 633 Initial PRR5 levels were taken from Fig. 5D at t=12 hours (initial dark).

- Values for k_3 are derived from experimental values for the adduct decay time constant
- 636 (τ) present in table 1, where $k_3=1/\tau$.
- Results were plotted in Figure 5—supplement 2.

Cloning and Purification:

ZEITLUPE construct ZTL-S composed of residues 29-165 were cloned into both p-His and pGST parallel vectors using Ncol and Xhol restriction sites. Proteins were purified as reported previously (13) . These DNA sequences were verified by GENEWIZ sequencing service. The plasmids were then isolated and tested for protein expression. All constructs were transformed into E. coli (JM109 or JM109DE3) cells and grown overnight at 37°C as starter culture till $O.D_{600} \sim 0.6$ -0.7. The rich culture was then transferred into 1.0 L of LB media for large-scale expression. These cultures were grown for 2-3 hr at 37°C till $O.D_{600} \sim 0.5$ -0.6 then the temperature was lowered to 18°C. The culture was then induced with 200 μM Isopropyl-β-D-thio-galactopyranoside (IPTG) after 1 hr incubation at 18°C. After induction, the cells were grown at 18°C for about 18-20 hr. Finally, the cells were centrifuged at 4000 rpm to collect and store the cells in stabilizing buffer (50mM Tris pH 7or 50mM Hepes pH 8 with 100mM and 10% glycerol). The harvested cell-pellets were stored for later use at -80°C.

We note that ZTL is difficult to express and purify from *E. coli* as most WT proteins are confined to inclusion bodies. Typical experiments required cell pellets from 18 L of cells. Such

difficulties make studies of variants such as G46S difficult in the absence of G80R. The G80R variant, likely due to the stabilizing effects of the R80-F84 π -cation interaction (Figure 2B), enhances protein yields in *E. coli* substantially. This allows access to G46S:G80R, despite intractable yields of the isolated G46S variant.

ZTL-S was purified using affinity chromatography followed by size exclusion chromatography. Prior to purification the cells were lysed by sonication at 4°C. After sonication the protein solution was centrifuged at 18k rpm at 4°C for 60 min. The supernatant was then purified using Ni-NTA or GST affinity columns. 6xHis and GST tags were cleaved using 6His-TEV-protease followed by an additional round of Ni-NTA affinity chromatography to remove the 6His tag and 6His-TEV-protease. The final eluted protein was subjected to Fast Protein Liquid Chromatography (FPLC) using a Hiload Superdex 200 16/60 gel filtration column equilibrated with stabilizing buffer.

Size Exclusion Chromatography

Solution characterization of purified proteins was done using a Superdex 200 10/300 analytical column (GE Lifesciences). Protein concentrations were determined using the absorbance at 450 nm (ext. coefficient 12,500). Apparent molecular weights were calculated by comparing the elution volume of known standards (sweet potato β-amylase (200 kDa)-12.4 ml; yeast alcohol dehydrogenase (150 kDa)-13.31 ml; bovine albumin (66 kDa)-14.61 ml; carbonic anhydrase (29 kDa)-17.03 ml; horse heart cyctochrome c (12.4 kDa)-18.32 ml)) (Sigma Aldrich). Absolute molecular weights of ZTL 16-165, ZTL 29-165 and FKF1 28-174 were determined by subjecting samples to refractive index and light-scattering detectors on a Wyatt Minidawn light-scattering instrument following a Superdex 200 10/300 analytical column. MW's were determined using ASTRA software from Wyatt Technologies. All SEC and multi-angle light scattering experiments were conducted in stabilizing buffer (see above).

Mutagenesis:

Site specific protein variants of ZTL-S constructs were obtained using the quickchange protocol. Following PCR amplification samples were treated with 1 μ L of *DpnI* and incubated at 37°C for 2.5-3 hr to cleave the methylated template DNA. A single colony of DH5 α *E. coli* was grown at 37°C overnight and plasmid DNA was isolated and verified by DNA sequencing (Genewiz). Rate altering variants of ZTL were expressed, purified and characterized using the method described above.

Structural Analysis

ZTL-S and its variants were initially screened with Hampton Screens (HR2-110 and HR2-112) via the hanging drop methods using 1.5 μ L well solution with 1.5 μ L of ZTL-S at various concentration range of 5-10 mg/ml. Optimum crystallization conditions for WT (0.1 M Tris pH 8.5, 0.1 M Magnesium Chloride hexahydrate, 28% w/v PEG 4k), G80R (0.1 M Tris pH 8.5, 0.2 M Magnesium Chloride hexahydrate, 30% w/v PEG 4k), V48I:G80R (0.1 M Tris ph 8.5, 0.2 M Sodium Acetate trihydrate, 30% w/v PEG 4K). Protein for crystallographic studies was purified in the same stabilizing buffer.

Light state crystals of V48I:G80R were obtained as follows. Prior to setting screens V48I:G80R protein was exposed to a broad spectrum white flood light (150 W), while on ice for two minutes. Saturation of the light-state was confirmed by UV-vis spectra analysis, by verifying disappearance of the 450 and 478 nm absorption bands characteristic of the dark-state protein. The light-state protein was then crystallized directly using the hanging drop method outlined above. Crystals appeared within 24 hours, and trays were exposed to white light once a day to maintain population of the light-state species.

Diffraction data was collected at the F1 beamline at the Cornell High-Energy Synchrotron Source (CHESS). Data for WT and all variants was collected at 100 K. The following cryoprotectants were added: V48I:G80R dark (25% Glycerol v/v), V48I:G80R light (25% Glycerol v/v), G80R (25% ethylene glycol v/v), and WT (25% ethylene glycol v/v). Data was

scaled and reduced in HKL2000 (53) (see S2 for refinement statistics). The initial WT structure was solved using molecular replacement in PHASER (54) and PHENIX (55) with the LOV1 domain of *Arabidopsis* phototropin 2 (PDBID 2Z6D) as a search model. Structures of ZTL variants were solved using the same method with WT ZTL as the search model. Rebuild cycles were completed in COOT (56) and refinement with REFMAC5 (57) and PHENIX (55). All ZTL structures contain four molecules per asymmetric unit that is composed of two anti-parallel LOV dimers. Residues 29-31 are not visible in the electron density in any molecule. In several molecules residues 29-43 and 164-165 are unable to be resolved and have not been built. For light-state structures clear density is observed for the adduct state in two of four molecules. Although electron density suggests an adduct for the remaining two molecules, we do not model them with an adduct and the reduced density likely reflects reduction by x-rays during data collection as has been observed previously (6).

UV-absorption spectroscopy and kinetics:

Purified protein fractions were concentrated to 30-60 μ M for UV-Vis absorption spectroscopy measurements and kinetics. Samples were exposed to a broad spectrum white flood light (150 W), while on ice for two minutes. An Agilent UV3600 spectrophotometer was used to characterize the absorption spectra of all constructs in both light and dark states. The light state peak of 378nm (ext. coefficient 8,500) and dark state peak 450nm (ext. coefficient 12,500) were used to estimate the protein concentrations for experiments.

Photocycle recovery kinetics were analyzed by measuring the absorption at 450 and 478 nm as a function of time. Spectra were collected at intervals ranging from 100 seconds-2 hours to ensure minimal repopulation of the light-state by the probe source. Time intervals were chosen to maintain approximately 10-20 measurements per half life. Kinetic traces at 450 and 478 nm were then fit with a monoexponential decay of the form $y=y_0+A^*e^{-k^*x}$. The rate constant k and time constant (1/k) were abstracted. Results are presented in table 1 as the average of three independent measurements.

Plant materials and growth conditions

730

731 The Columbia-0 (Col-0) plant that possesses CCA:LUC reporter was previously described (58). 732 To generate overexpressors of HA-ZTL, HA-ZTL (V48I), HA-ZTL(G80R) and HA-ZTL 733 (V48IG80R), the nucleotide sequences encoding HA tag was incorporated into the ZTL forward 734 primer (5'-CACCATGTACCCATACGATGTTCCAGATTACGCTGAGTGGGACAGTGGTTC-3', 735 the underline indicates the sequences that encodes HA tag). Amino acid substitutions on ZTL 736 coding region were generated by using megaprimer-based PCR amplification method (59). The 737 primers used for generating the mutated ZTL coding sequence are followings: ZTL (V48I) R (5'-738 AACGGCATCAGTAACAATGAATCCACAAGGCGC-3'), ZTL (G80R) R (5'-739 CAAGAAGCGGCAATTTCGTCCGAGAACTTCCTC-3'), ZTL R (5'-740 TTACGTGAGATAGCTCGCTA-3'). Amplified PCR fragments were cloned into pENTR/D-TOPO 741 vector (Invitrogen). After verifying sequences, HA-ZTL and mutated HA-ZTL coding regions 742 were transferred into pB7WG2 or pH7WG2 binary vector (60) using LR Clonase II enzyme mix 743 (Invitrogen) to generate 35S:HA-ZTL, 35S:HA-ZTL (V48I), 35S:HA-ZTL (G80R) and 35S:HA-744 ZTL (V48I:G80R). The binary vectors were introduced into the CCA1:LUC plants by 745 conventional Agrobacterium-mediated transformation method. The T3 generations of transgenic 746 lines in which the expression levels of ZTL variant mRNAs were similar were chosen for the 747 circadian analysis. The plants were grown on soil or Linsmaier and Skoog (LS) media (Caisson) 748 in plant incubator (Percival Scientific) set at 22°C under full-spectrum white fluorescent light (70-90 µmol m⁻²s⁻¹: F017/950/24", Octron Osram Sylvania) in long days (16-h light/8-h dark). 749

Bioluminescence Imaging

750

751

752

753

754

755

Bioluminescence Imaging and analysis were performed as previously described with minor modifications (61). Seedlings were grown on LS media in the plant incubator (Percival Scientific) in 12-h light/12-h dark photoperiod for 10 days before being transferred to continuous light (40-50 µmol m⁻²s⁻¹) conditions. 9-day-old seedlings were pretreated with 5 mM D-luciferin (Biosynth) in 0.01% Triton X-100 solution, and incubated one day before imaging. The bioluminescence

756

757

758

759

760

761

762

763

764

765

766

767

768

769

770

771

772

773

774

775

776

777

778

779

780

Co-immunoprecipitation assays

generated from the CCA1:LUC reporter was imaged for 15 minutes at every 2 hours using NightOwl system (Berthold) and analyzed using IndiGO software (Berthold). Period length estimation was performed using fast Fourier Transform-Nonlinear Least Squares (FFT-NLLS) analysis in the Biological Rhythms Analysis Software System (BRASS) (http://millar. bio.ed.ac.uk/PEBrown/BRASS/BrassPage.htm). RNA isolation and gene expression analysis For gene expression analyses, 14-day-old seedlings grown on LS agar plates were harvested at ZT16 and used for RNA extraction using illustra RNAspin Mini kit (GE Healthcare). 2 µg of RNA was reverse-transcribed using iScript cDNA synthesis kit (Bio-Rad). The cDNA was diluted by adding 40 µL of water, and 2 µL of cDNA was used for quantitative polymerase chain reaction (g-PCR) using MyiQ real-time thermal cycler (Bio-Rad). IPP2 expression was used as an internal control to normalize cDNA amount. Primers and PCR conditions used for IPP2, PRR5, TOC1 and ZTL amplification were previously described (17). Expression of ZTL, PRR5 and *TOC1* was calculated from three biological replicates. Western blots To analyze the expression levels of HA fused ZTL protein, endogenous PRR5, and TOC1 proteins, seedlings were grown in 12-h light/12-h dark conditions for 14 days. Total protein was extracted using extraction buffer [50 mM Na-P pH7.5, 150 mM KCl, 1 mM DTT, 1 mM EDTA, 0.05% Sodium deoxycholate, 0.1% SDS, 50 µM MG-132, Protease inhibitor cocktail (Pierce)}. Protein was separated in 9% SDS-PAGE gels and transferred to Nitrocellulose membrane (Bio-Rad). HA-ZTL and Actin were detected using anti-HA (3F10, Roche) and anti-actin (C4, Millipore) antibodies, respectively. Western procedure for detecting TOC1 and PRR5 proteins was previously described (17). For protein quantification, western blot images were analyzed using Image J (62).

For Figure 4—figure supplement 1A, *Agrobacteria* containing both GI and ZTL variants were coinfiltrated into 4-week-old *N. benthamiana* leaves. The infiltrated plants were incubated under LD for two days and transferred to continuous light or dark with additional 24 h incubation. Co-IP was performed according to Fujiwara et al (28). The immuno-complexes were resuspended in SDS sample buffer and heated briefly. GFP antibody (Invitrogen, A11120) was used for immunoprecipitation of GI-GFP protein. ZTL variants were detected by western blotting with HA antibody. For Figure 4—figure supplement 1B, *Agrobacterium* harboring each overexpression construct was mixed according to combinations indicated and was infiltrated into 3-week-old *N. benthamiana* leaves and incubated in LD and either light or darkness as described above. Sample preparation, the IP buffer condition, the IP method and immunoblot procedure were described previously (22).

792

793

781

782

783

784

785

786

787

788

789

790

791

References:

- Lokhandwala J, et al. (2015) Structural Biochemistry of a Fungal LOV Domain
 Photoreceptor Reveals an Evolutionarily Conserved Pathway Integrating Light and
 Oxidative Stress. Structure 23(1):116-125.
- Sahar S & Sassone-Corsi P (2009) Metabolism and cancer: the circadian clock
 connection. *Nat Rev Cancer* 9(12):886-896.
- Taylor B & Zhulin IB (1999) PAS Domains: Internal Sensors of Oxygen, Redox Potential, and Light. *Micro. Mol. Biol. Rev.* 63(2):479-506.
- Haizumi T, Tran HG, Swartz TE, Briggs WR, & Kay SA (2003) FKF1 is essential for photoperiodic-specific light signalling in Arabidopsis. *Nature* 426(6964):302-306.
- Somers DE, Schultz TF, Milnamow M, & Kay SA (2000) ZEITLUPE encodes a novel clock-associated PAS protein from Arabidopsis. *Cell* 101(3):319-329.
- 805 6. Zoltowski BD, *et al.* (2007) Conformational Switching in the Fungal Light Sensor Vivid.
 806 Science 316:1054-1057.

807	7.	Pudasaini A, El-Arab KK, & Zoltowski BD (2015) LOV-based optogenetic devices: light-
808		driven modules to impart photoregulated control of cellular signaling. Front Mol Biosci
809		2:18.
810	8.	Harper SM, Christie JM, & Gardner KH (2004) Disruption of the LOV-Jalpha Helix
811		Interaction Activates Phototropin Kinase Activity. Biochemistry 43:16184-16192.
812	9.	Jones MA, Feeney KA, Kelly SM, & Christie JM (2007) Mutational analysis of
813		phototropin 1 provides insights into the mechanism underlying LOV2 signal transmission
814		J Biol Chem 282(9):6405-6414.
815	10.	Salomon M, Christie JM, Knieb E, Lempert U, & Briggs WR (2000) Photochemical and
816		mutational analysis of the FMN-binding domains of the plant blue light receptor,
817		phototropin. Biochemistry 39(31):9401-9410.
818	11.	Zoltowski BD & Gardner KH (2011) Tripping the Light Fantastic: Blue-Light
819		Photoreceptors as Examples of Environmentally Modulated Protein-Protein Interactions.
820		Biochemistry 50(1):4-16.
821	12.	Kennis JTM, et al. (2004) The LOV2 domain of phototropin: A reversible photochromic
822		switch. Journal of the American Chemical Society 126(14):4512-4513.
823	13.	Pudasaini A & Zoltowski BD (2013) Zeitlupe senses blue-light fluence to mediate
824		circadian timing in Arabidopsis thaliana. Biochemistry 52:7150-7158.
825	14.	Halavaty A & Moffat K (2007) N- and C-Terminal Flanking Regions Modulate Light-
826		Induced Signal Transduction in the LOV2 Domain of the Blue Light Sensor Phototropin 1
827		from Avena Sativa. Biochemistry 46(49):14001-14009.
828	15.	Harper SM, Neil LC, & Gardner KH (2003) Structural Basis of a Phototropin Light Switch.
829		Science 301:1541-1544.
830	16.	Zoltowski BD, Motta-Mena LB, & Gardner KH (2013) Blue light-induced dimerization of a
831		bacterial LOV-HTH DNA-binding protein. <i>Biochemistry</i> 52(38):6653-6661.

832	17.	Baudry A, et al. (2010) F-Box Proteins FKF1 and LKP2 Act in Concert with ZEITLUPE to
833		Control Arabidopsis Clock Progression. Plant Cell 22(3):606-622.
834	18.	Zoltowski BD & Imaizumi T (2014) Structure and Function of the ZTL/FKF1/LKP2 Group
835		Proteins in Arabidopsis. <i>Enzymes</i> 35:213-239.
836	19.	Mas P, Kim WY, Somers DE, & Kay SA (2003) Targeted degradation of TOC1 by ZTL
837		modulates circadian function in Arabidopsis thaliana. <i>Nature</i> 426(6966):567-570.
838	20.	Imaizumi T, Schultz TF, Harmon FG, Ho LA, & Kay SA (2005) FKF1F-BOX protein
839		mediates cyclic degradation of a repressor of CONSTANS in Arabidopsis. Science
840		309(5732):293-297.
841	21.	Sawa M, Nusinow DA, Kay SA, & Imaizumi T (2007) FKF1 and GIGANTEA complex
842		formation is required for day-length measurement in Arabidopsis. Science
843		318(5848):261-265.
844	22.	Song YH, Smith RW, To BJ, Millar AJ, & Imaizumi T (2012) FKF1 conveys timing
845		information for CONSTANS stabilization in photoperiodic flowering. Science
846		336(6084):1045-1049.
847	23.	Song YH, et al. (2014) Distinct roles of FKF1, Gigantea, and Zeitlupe proteins in the
848		regulation of Constans stability in Arabidopsis photoperiodic flowering. Proc Natl Acad
849		Sci U S A 111(49):17672-17677.
850	24.	Kim J, Geng R, Gallenstein RA, & Somers DE (2013) The F-box protein ZEITLUPE
851		controls stability and nucleocytoplasmic partitioning of GIGANTEA. Development
852		140(19):4060-4069.
853	25.	Kim WY, et al. (2007) ZEITLUPE is a circadian photoreceptor stabilized by GIGANTEA
854		in blue light. <i>Nature</i> 449(7160):356-360.
855	26.	Somers DE, Kim WY, & Geng RS (2004) The F-box protein ZEITLUPE confers dosage-
856		dependent control on the circadian clock, photomorphogenesis, and flowering time.

857

Plant Cell 16(3):769-782.

858	27.	Kiba T, Henriques R, Sakakibara H, & Chua NH (2007) Targeted degradation of
859		PSEUDO-RESPONSE REGULATOR5 by an SCFZTL complex regulates clock function
860		and photomorphogenesis in Arabidopsis thaliana. <i>Plant Cell</i> 19(8):2516-2530.
861	28.	Fujiwara S, et al. (2008) Post-translational regulation of the Arabidopsis circadian clock
862		through selective proteolysis and phosphorylation of pseudo-response regulator proteins.
863		Journal of Biological Chemistry 283(34):23073-23083.
864	29.	Mas P, Alabadi D, Yanovsky MJ, Oyama T, & Kay SA (2003) Dual role of TOC1 in the
865		control of circadian and photomorphogenic responses in Arabidopsis. Plant Cell
866		15(1):223-236.
867	30.	De Caluwe J, et al. (2016) A Compact Model for the Complex Plant Circadian Clock.
868		Front Plant Sci 7:74.
869	31.	Pokhilko A, Mas P, & Millar AJ (2013) Modelling the widespread effects of TOC1
870		signalling on the plant circadian clock and its outputs. BMC Syst Biol 7:23.
871	32.	Dasgupta A, et al. (2015) Biological Significance of Photoreceptor Photocycle Length:
872		VIVID Photocycle Governs the Dynamic VIVID-White Collar Complex Pool Mediating
873		Photo-adaptation and Response to Changes in Light Intensity. PLoS Genet
874		11(5):e1005215.
875	33.	Zoltowski BD, Vaccaro B, & Crane BR (2009) Mechanism-based tuning of a LOV
876		domain photoreceptor. Nat Chem Biol 5(11):827-834.
877	34.	El-Arab KK, Pudasaini A, & Zoltowski BD (2015) Short LOV Proteins in Methylocystis
878		Reveal Insight into LOV Domain Photocycle Mechanisms. <i>PLoS One</i> 10(5):e0124874.
879	35.	Christie JM, et al. (2007) Steric Interactions Stabilize the Signaling State of the LOV2
880		Domain of Phototropin 1. Biochemistry 46:9310-9319.
881	36.	Lokhandwala J, et al. (2016) A Native Threonine Coordinates Ordered Water to Tune
882		Light-Oxygen-Voltage (LOV) Domain Photocycle Kinetics and Osmotic Stress Signaling
883		in Trichoderma reesei ENVOY. J Biol Chem 291(28):14839-14850.

884	37.	Strickland D, et al. (2012) TULIPs: tunable, light-controlled interacting protein tags for
885		cell biology. Nat Methods 9(4):379-384.
886	38.	Ito S, Song YH, & Imaizumi T (2012) LOV domain-containing F-box proteins: light-
887		dependent protein degradation modules in Arabidopsis. <i>Molecular plant</i> 5(3):573-582.
888	39.	Nakasako M, Matsuoka D, Zikihara K, & Tokutomi S (2005) Quaternary structure of
889		LOV-domain containing polypeptide of Arabidopsis FKF1 protein. FEBS letters
890		579(5):1067-1071.
891	40.	Han L, Mason M, Risseeuw EP, Crosby WL, & Somers DE (2004) Formation of an
892		SCF(ZTL) complex is required for proper regulation of circadian timing. <i>Plant J</i>
893		40(2):291-301.
894	41.	Card PB, Erbel PJA, & Gardner KH (2005) Structural Basis of ARNT PAS-B
895		Dimerization: Use of a Common Beta-sheet Interface for Hetero- and Homodimerization
896		Journal of Molecular Biology 353:664-667.
897	42.	Lamb JS, et al. (2009) Illuminating solution responses of a LOV domain protein with
898		photocoupled small-angle X-ray scattering. J Mol Biol 393(4):909-919.
899	43.	Zoltowski BD & Crane BR (2008) Light Activation of the LOV Protein VVD Generates a
900		Rapidly Exchanging Dimer. Biochemistry 47:7012-7019.
901	44.	Moglich A & Moffat K (2007) Structural basis for light-dependent signaling in the dimeric
902		LOV domain of the photosensor YtvA. J Mol Biol 373(1):112-126.
903	45.	Partch CL, Card PB, Amezcua CA, & Gardner KH (2009) Molecular basis of coiled coil
904		coactivator recruitment by the aryl hydrocarbon receptor nuclear translocator (ARNT). J
905		Biol Chem 284(22):15184-15192.
906	46.	Freddolino PL, Gardner KH, & Schulten K (2013) Signaling mechanisms of LOV
907		domains: new insights from molecular dynamics studies. Photochemical &
908		photobiological sciences : Official journal of the European Photochemistry Association

and the European Society for Photobiology 12(7):1158-1170.

909

910	47.	Kim WY, Geng R, & Somers DE (2003) Circadian phase-specific degradation of the F-
911		box protein ZTL is mediated by the proteasome. Proc Natl Acad Sci U S A 100(8):4933
912		4938.
913	48.	Gendron JM, et al. (2012) Arabidopsis circadian clock protein, TOC1, is a DNA-binding
914		transcription factor. Proc Natl Acad Sci U S A 109(8):3167-3172.
915	49.	Vaidya AT, Chen CH, Dunlap JC, Loros JJ, & Crane BR (2011) Structure of a light-
916		activated LOV protein dimer that regulates transcription. Sci Signal 4(184):ra50.
917	50.	Nash AI, Ko WH, Harper SM, & Gardner KH (2008) A conserved glutamine plays a
918		central role in LOV domain signal transmission and its duration. Biochemistry
919		47(52):13842-13849.
920	51.	Nozaki D, et al. (2004) Role of Gln1029 in the Photoactivation Processes of the LOV2
921		Domain in Adiantum Phytochrome3. Biochemistry 43:8373-8379.
922	52.	Wang L, Fujiwara S, & Somers DE (2010) PRR5 regulates phosphorylation, nuclear
923		import and subnuclear localization of TOC1 in the Arabidopsis circadian clock. EMBO
924		29(11):1903-1915.
925	53.	Otwinowski Z & Minor W (1997) Processing of X-ray diffraction data collected in
926		oscillation mode. Macromolecular Crystallography, Pt A 276:307-326.
927	54.	Mccoy AJ, et al. (2007) Phaser crystallographic software. Journal of Applied
928		Crystallography 40:658-674.
929	55.	Adams PD, et al. (2010) PHENIX: a comprehensive Python-based system for
930		macromolecular structure solution. Acta Crystallogr D Biol Crystallogr 66(Pt 2):213-221
931	56.	Emsley P & Cowtan K (2004) Coot: model-building tools for molecular graphics. Acta
932		Crystallogr D Biol Crystallogr 60(Pt 12 Pt 1):2126-2132.

Murshudov GN, Vagin AA, & Dodson EJ (1997) Refinement of macromolecular

structures by the maximum-likelihood method. Acta Crystallogr D Biol Crystallogr 53(Pt

933

934

935

57.

3):240-255.

936	58.	Pruneda-Paz JL (2009) A functional genomics approach reveals CHE as a component of
937		the Arabidopsis circadian clock (vol 325, pg 1481, 2009). <i>Science</i> 326(5951):366-366.
938	59.	Burke E & Barik S (2003) Megaprimer PCR: application in mutagenesis and gene fusion.
939		Methods Mol Biol 226:525-532.
940	60.	Karimi M, Inze D, & Depicker A (2002) GATEWAY vectors for Agrobacterium-mediated
941		plant transformation. Trends Plant Sci 7(5):193-195.
942	61.	Fenske MP, et al. (2015) Circadian clock gene LATE ELONGATED HYPOCOTYL
943		directly regulates the timing of floral scent emission in Petunia. Proc Natl Acad Sci U S A
944		112(31):9775-9780.
945	62.	Schneider CA, Rasband WS, & Eliceiri KW (2012) NIH Image to ImageJ: 25 years of
946		image analysis. Nat Methods 9(7):671-675.
947	63.	Rzhetsky A & Nei M (1992) A simple method for estimating and testing minimum
948		evolution trees. <i>Molecular Biology and Evolution</i> 9:945-967.
949	64.	Felsenstein J (1985) Confidence limits on phylogenies: An approach using the bootstrap.
950		Evolution 39(4):783-791.
951	65.	Zuckerkandl E & Pauling L (1965) Evolutionary divergence and convergence in proteins.
952		Evolving Genes and Proteins, eds Bryson V & Vogel HJ (Academic Press, New York),
953		pp 97-166.
954	66.	Nei M & Kumar S (2000) Molecular Evolution and Phylogenetics (Oxford University
955		Press, New York).
956	67.	Saitou N & Nei M (1987) The neighbor-joining method: a new method for reconstructing
957		phylogenetic trees. Mol Biol Evol 4(4):406-425.
958	68.	Tamura K, Dudley J, Nei M, & Kumar S (2007) MEGA4: Molecular Evolutionary Genetics
959		Analysis (MEGA) software version 4.0. Mol Biol Evol 24(8):1596-1599.
960		

Figure Legends

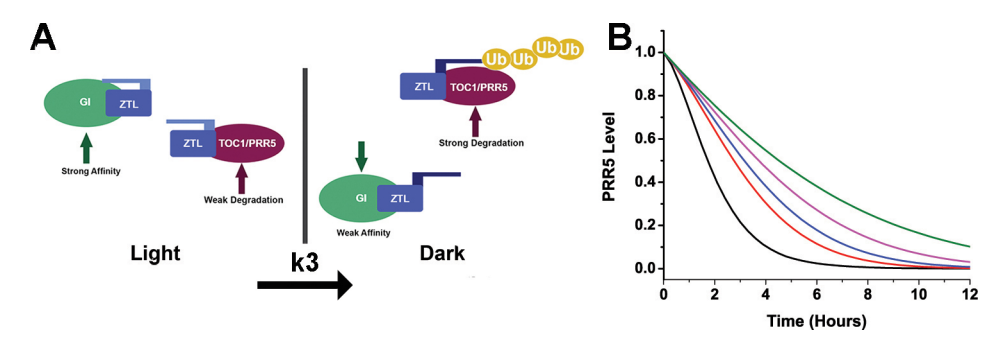


Figure 1. Models of ZTL photochemistry and regulation of circadian period. A) In the light, ZTL associates with both GI and degradation targets (PRR5/TOC1). During the day, the strong affinity for GI allows GI, ZTL, TOC1 and PRR5 levels to rise. Upon dusk, the adduct form of ZTL decays with a rate constant k_3 , leading to a conformational change. The conformation change decreases GI affinity and leads to ubiquitination of ZTL targets. B) Modeling PRR5 degradation as a function of k_3 (see equation 1 and methods for model generation and parameter selection). Using k_3 for WT (black), G80R (red), V48I (blue), G46S:G80R (magenta) and V48I:G80R (green) leads to predictable changes in PRR5 degradation patterns. (Figure supplements 1,2,3).

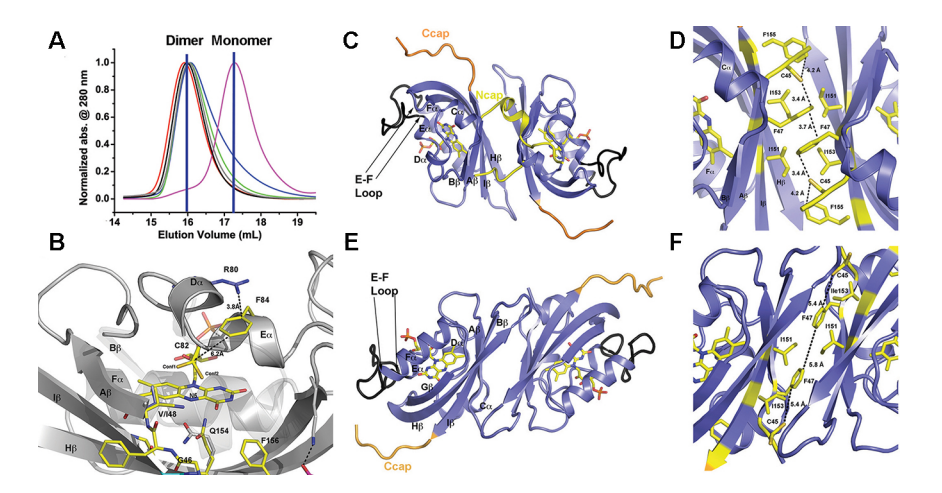


Figure 2. Structural analysis and LOV dimer formation in ZTL (A) G80R (dark-state, black; light-state (grey), WT (red), V48I:G80R (green), G46S:G80R (blue) all elute as dimers with apparent MWs of 38-41 kDa compared to the expected monomer of 16 kDa. Multi-Angle-Light-

977

978

979

980

981

982

983

984

985

986

987

988

989

990

991

992

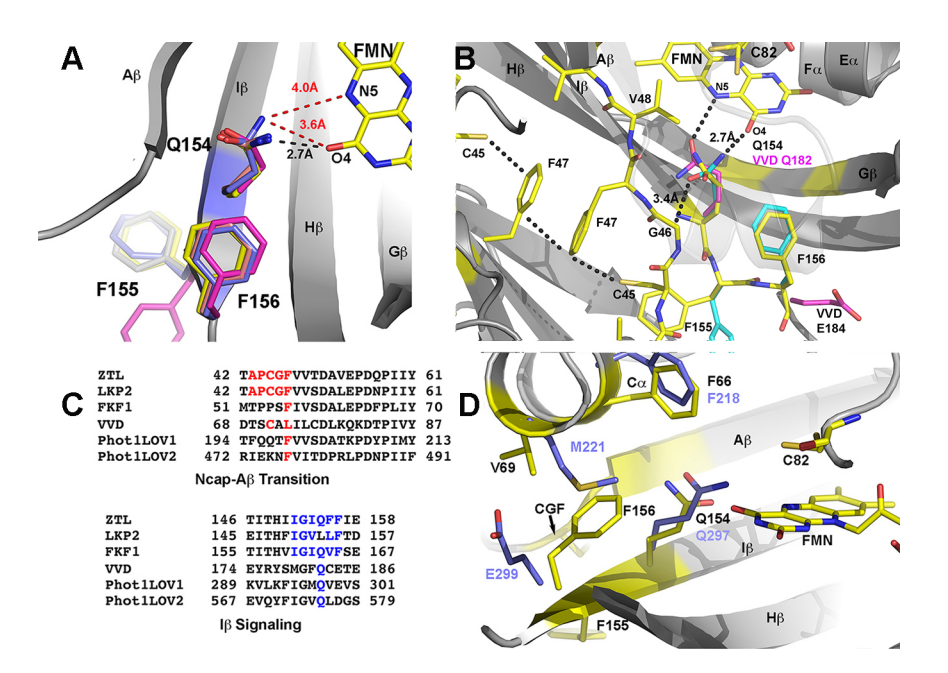
993

994

995

996

Scattering (MALS) confirms dimer formation in WT 29-165 (absolute MW 33 +/- 2 kDa) and 16-165 constructs (See Fig. 2 supplement 1). Introduction of an I151R abolishes dimer formation (magenta; apparent MW=22 kDa). (B) Structure of ZTL active site (yellow) and residues involved in structural or kinetic modulation of signaling (purple). R80 within D α forms a π -cation interaction with F84 directly above the photoreactive C82, resulting in steric stabilization of adduct formation. The observed steric stabilization through the π -cation interaction is consistent with the longer photocycle in G80R. V48I positions the additional methyl group into a pocket adjacent to N5, C82 and Q154. Comparisons of AsLOV2 structures (white; buried conformation), dark-state ZTL (yellow; exposed conformation) demonstrates that V48I can impact the position of Q154 between buried and exposed conformations. Movement of Q154 correlates with movement of F156 in Iβ. (C-F) ZTL monomers are defined by an antiparallel βsheet flanked by a series of α -helices (C α , D α , E α , F α). The helices cradle the photoreactive FMN adjacent to C82 (E α helix). ZTL contains a 9-residue insert linking the E-F helices that accommodates the adenine ring of FAD in some LOV proteins (black) (6). N- and C-terminal extensions (Ncap/Ccap; yellow) are largely disordered; however, a short helix within the Ncap reaches across a dimer interface in some molecules to form contacts between the C α and D α helices. Two dimer interfaces are formed through the β-scaffold in ZTL. The compact dimer (C,D) differs from the elongated dimer (E,F) by a 2.0 Å translation along the β-sheet. Key residues in the dimer interface are shown in yellow. The translation disrupts a network of sulfur- π and π - π interactions involving C45 and F47, centered around I151. (Figure supplements 1.2).



997

998

999

1000

1001

1002

1003

1004

1005

1006

1007

1008

1009

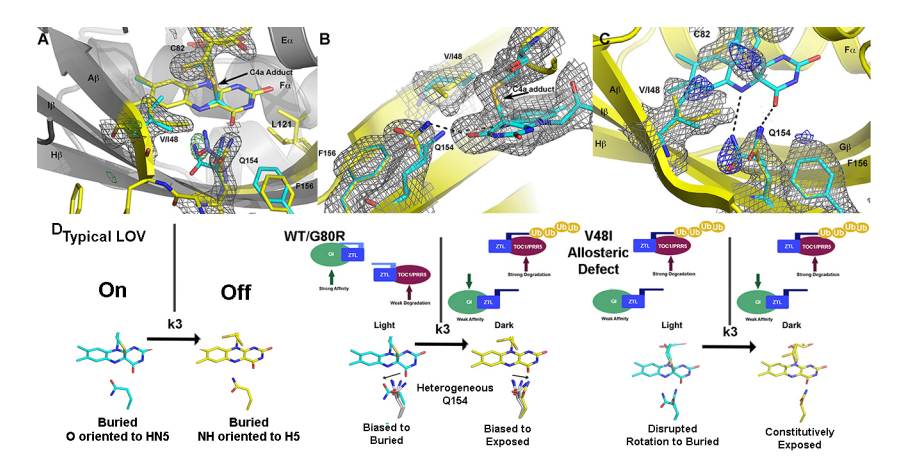
1010

1011

1012

Figure 3: Q154 links Ncap, Ccap and helical elements. (A) Q154 exists in multiple conformations in WT ZTL structures. They differ in interactions with the active site flavin. An exposed conformation forms strong H-bonds to the O4 position (black dotted line). A buried conformation forms weaker interactions (3.6 Å) with O4 that leads to closer interactions at N5 (4.0 Å; red dotted line). The altered conformation is coupled to movement of F156 into the active site and multiple conformations of F155, forming a QFF motif. The altered conformations define ZTL signaling as distinctly different than existing LOV structures. (B) The unusual orientations of Q154 differ from other LOV proteins that typically show strong interactions near N5 (VVD; magenta). The heterogeneous conformations of Q154 directly abut G46 in a CGF motif allowing formation of the sulfur- π and π - π interactions involving C45 and F47. F156 then adopts a buried conformation in contrast to the equivalent residue in VVD (E184) (C) Sequence alignments of LOV proteins depict conserved elements within the CGF motif (red) and QFF motif (blue) in Arabidopsis thaliana ZTL, LKP2, FKF1, phototropin 1 LOV1 and LOV2. Sequence conservation indicates divergent signaling mechanisms within the ZTL/FKF1 family compared to existing LOV allostery models. (D) Comparisons of ZTL (yellow, black lettering) and Arabidopsis thaliana phototropin 1 LOV1 (PDB: 2Z6C; blue). The altered conformation of Q154 draws F156

into the active site. The buried conformation of F156, leads to movement of $C\alpha$ (F66, V69). (Figure supplements 1).



1016

1017

1018

1019

1020

1021

1022

1023

1024

1025

1026

1027

1028

1029

1030

1031

1032

1014

Figure 4: Structural effects on ZTL chemistry and signaling. (A) Comparison of dark-state V48I:G80R (yellow), light-state V48I:G80R (cyan) and dark-state AtLOV1 phototropin 1 (purple: PDB ID: 2Z6C) molecules. 2Fo-Fc (2.0 σ grey mesh) and Fo-Fc (3.0 σ green mesh) are depicted for dark-state V48I:G80R. Lack of density for an adduct is consistent with minimal population of the light-state species. Density shows clear selection of the I48 methyl group towards Q154. Some residual density is present in the buried conformation of Q154 that indicates either partial occupancy of the site in the dark, or residual light-state conformations. The buried conformation correlates with the orientation of Q154 in all other LOV structures as depicted by AsLOV2. Electron density for FMN is excluded to allow clear observation of electron density for active site side-chains. (B) Light state crystal structure of V48I:G80R, 2Fo-Fc data shown at 2.0 σ show (grey mesh) clear electron density for C4a adduct formation. (C) Rotated view of the active site of the light-state ZTL molecule. Modeling of Q154 in the exposed conformation (yellow; panel C) results in Fo-Fc (blue mesh; panel C) density at 3.0 σ for the light-state molecule. Electron density for the FMN is excluded for clarity. The data confirms rotation of Q154 to a buried conformation (cyan) following adduct formation. Rotation of Q154 is coupled to rearrangement of V/I48. In V48I, the additional methyl groups blocks rotation,

partially inhibiting population of the buried conformation of Q154 (cyan conformation). D) Predicted divergent ZTL model of allostery and signal transduction based on the integrated structural, mutational and *in vivo* data. Orientations of WT/G80R Q154 are derived from the dark-state G80R ZTL structure with buried and exposed conformations shown for reference from V48I:G80R. WT/G80R and V48I:G80R deviate from typical LOV models (derived from VVD: light PDBID 3RH8, dark PDBID 2PD7) on the position of Q154. WT/G80R ZTL retains a heterogeneous orientation of Q154. We propose that Q154 is heterogeneous regardless of lighting conditions, but biased towards the buried conformation in the light. At dusk adduct decay, with rate constant k₃, causes the Q154 conformation to be biased towards an exposed conformation, accelerating ubquitination of protein targets. For V48I, I48 selects the exposed conformation in the dark and leads to only partial burying of Q154 (shown in C, D), leading to constitutively high ubquitination activity that mimics the dark-state of WT-ZTL. (Figure supplements 1,2).

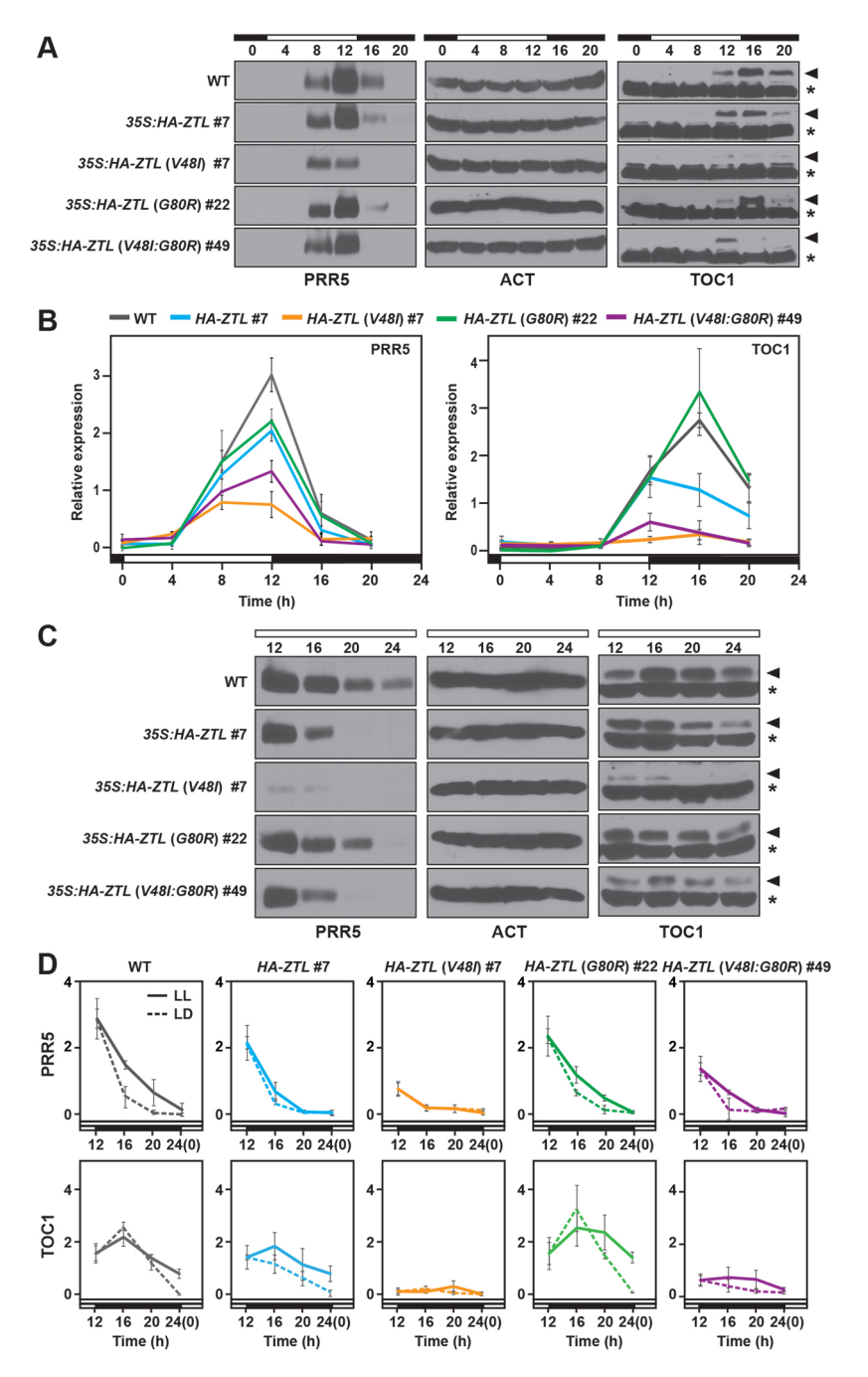


Figure 5. Diurnal and circadian expression profiles of PRR5 and TOC1 proteins in ZTL variant overexpressors. (A) PRR5 and TOC1 protein levels were analyzed in WT, 35S: HA-ZTL, 35S: HA-ZTL (V48I), 35S: HA-ZTL (G80R) and 35S: HA-ZTL (V48I:G80R) under 12L/12D conditions. Actin (ACT) was used as a loading control for PRR5. Arrowhead indicates the band corresponding to TOC1 protein, while an asterisk indicates a nonspecific cross-reacting band,

which is used as a loading control. (B) Relative expression level of PRR5 and TOC1 were determined in WT, 35S: HA-ZTL, 35S: HA-ZTL (V48I), 35S: HA-ZTL (G80R) and 35S: HA-ZTL (V48I:G80R) under 12L/12D conditions. Actin and the TOC1 nonspecific bands were used for normalizing protein loadings for quantification of PRR5 and TOC1. The data represent the averages ±SEM obtained from three biological replicates. (C) PRR5 and TOC1 protein levels were analyzed in WT, 35S: HA-ZTL, 35S: HA-ZTL (V48I), 35S: HA-ZTL (G80R) and 35S: HA-ZTL (V48I:G80R) during the subjective night under constant light conditions. (D) Relative levels of PRR5 and TOC1 proteins were determined in WT, 35S: HA-ZTL, 35S: HA-ZTL (V48I), 35S: HA-ZTL (G80R) and 35S: HA-ZTL (V48I:G80R). Dashed lines represent protein levels under 12L/12D conditions, while solid lines represent protein levels under constant light conditions. The data represent the averages ±SEM obtained from three biological replicates. (Figure supplements 1,2).

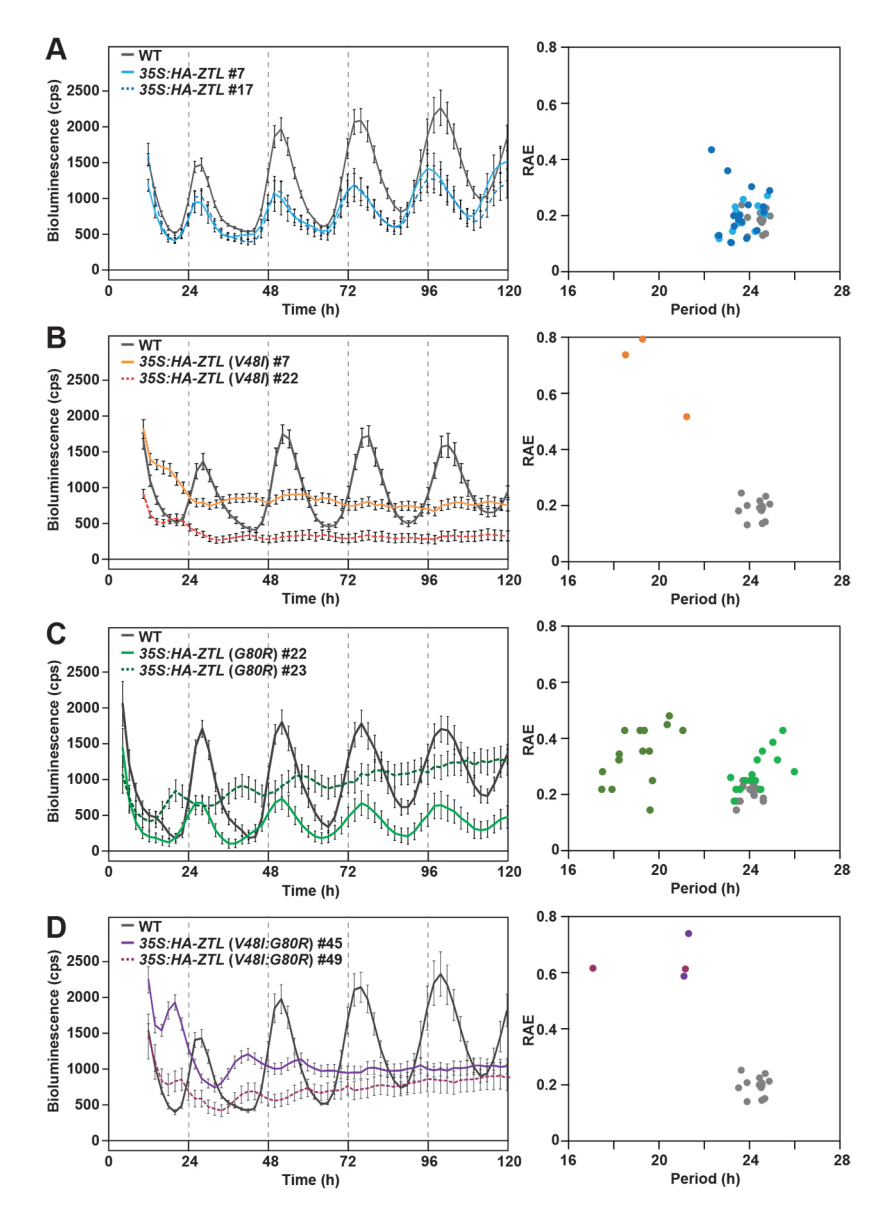


Figure 6. Circadian clock phenotypes of *ZTL* variant overexpressors. (A-D) *CCA1:LUC* activity was analyzed in WT, *35S:HA-ZTL* (A), *35S:HA-ZTL* (V48I) (B), *35S:HA-ZTL* (G80R) (C) and *35S:HA-ZTL* (V48I:G80R) (D) lines under continuous light conditions. *CCA1:LUC* traces represent the averages ±SEM of the results obtained from eight individual seedlings. Period length estimation and relative amplification errors of 16 individual measurements are shown.

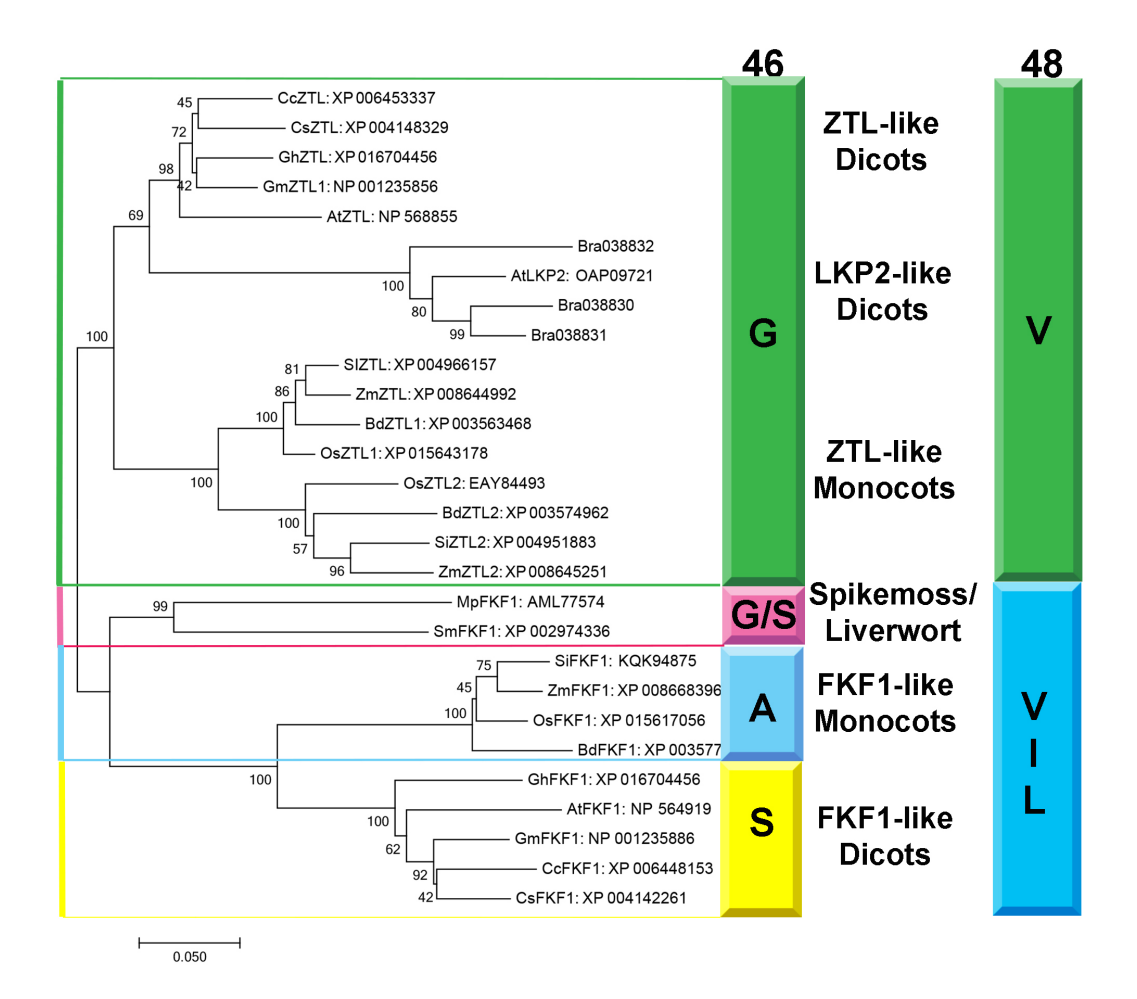


Figure 7: Phylogenetic Analysis of FKF1/ZTL family members in plants. Residue identity at position 46 (Colored Bar) distinguishes ZTL-like, LKP2-like and FKF1-like proteins consistent with evolutionary diversification of signaling mechanisms. LKP2 is isolated to a clade containing *Brassica rapa* members that all contain a Q154L substitution. Al ZTL members contain G46 which is necessary to promote the alternative conformation of Q154. Spikemoss and liverwort FKF1's are isolated indicating a possible intermediate function. Accession numbers for all sequences are shown after the protein name. The evolutionary history was inferred using the Minimum Evolution method (63). The percentage of replicate trees in which the associated taxa clustered together in the bootstrap test (500 replicates) are shown next to the branches (64).

The tree is drawn to scale, with branch lengths in the same units as those of the evolutionary distances used to infer the phylogenetic tree. The evolutionary distances were computed using the Poisson correction method (65) and are in the units of the number of amino acid substitutions per site. The ME tree was searched using the Close-Neighbor-Interchange (CNI) algorithm (66) at a search level of 1. The Neighbor-joining algorithm (67) was used to generate the initial tree. The analysis involved 28 amino acid sequences. All positions containing gaps and missing data were eliminated. There were a total of 535 positions in the final dataset. Evolutionary analyses were conducted in MEGA7 (68). (Figure supplements 1).

Figure Supplements

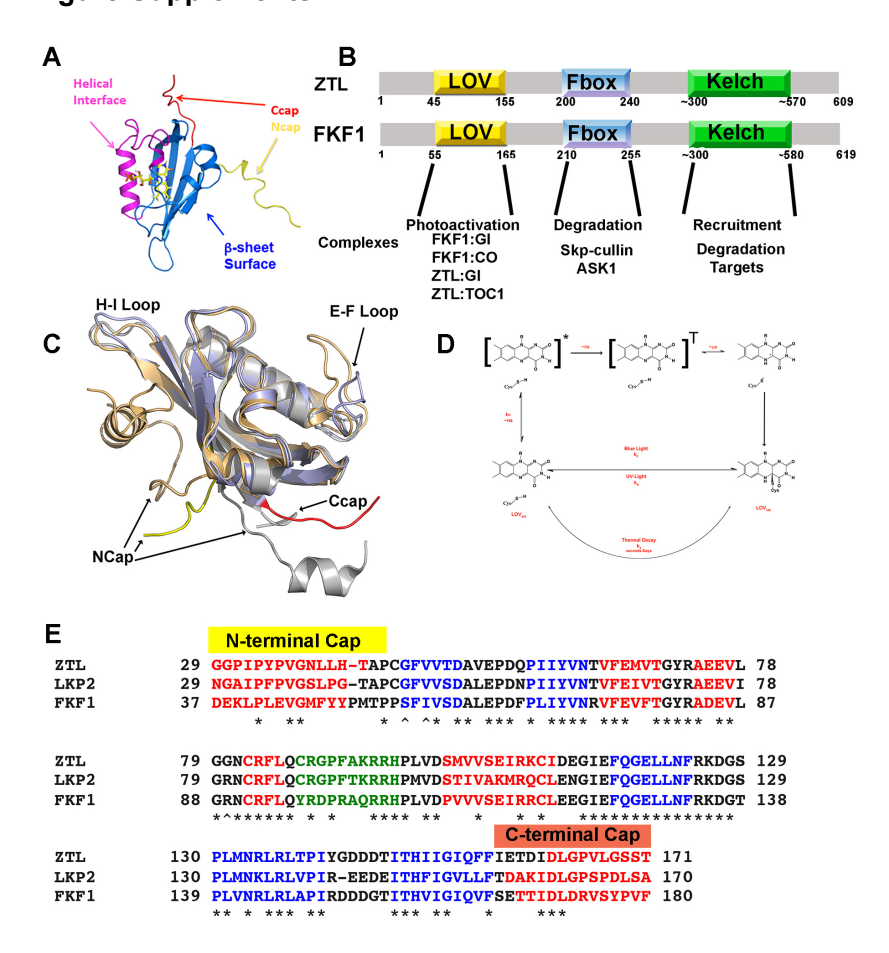


Figure 1—figure supplement 1. LOV chemistry and signal transduction. (A) PAS/LOV domains signal through 4 elements. Multi-domain proteins reorient Ncap (yellow) and Ccap

(red) elements to affect activity of signaling domains or recruit additional proteins to the PAS/LOV surface. The β -sheet (blue) and helical surface (magenta) act as protein:protein interactions motifs. (B) ZTL, and FKF1 domain architecture. The N-terminal LOV domain engages multiple targets. Light-activation then regulates Fbox activity to target proteins for degradation. (C) Superposition of VVD (light orange), AsLOV2 (grey) and ZTL. The ZTL LOV core (blue) is similar to existing LOV structures. Significant deviations exist at the Ncap (ZTL: Yellow), Ccap (ZTL: Red) and the E-F and H-I loops. These elements are believed to be important for signaling. (D) LOV proteins are activated by blue-light absorption to form an excited singlet state. The singlet rapidly undergoes intersystem crossing to generate a triplet intermediate. Proton coupled electron transfer from the conserved Cys residue and subsequent C4a adduct formation activates LOV proteins. The adduct state then decays in the dark or presence of UV-light. (E) Sequence alignment of ZTL family. Predicted helical regions (red), β -sheet (blue) and an extended E-F loop (green) are noted. * implies conserved, ^ residues tuning ZTL and FKF1 kinetics. The Ncap and Ccap regions are labeled.

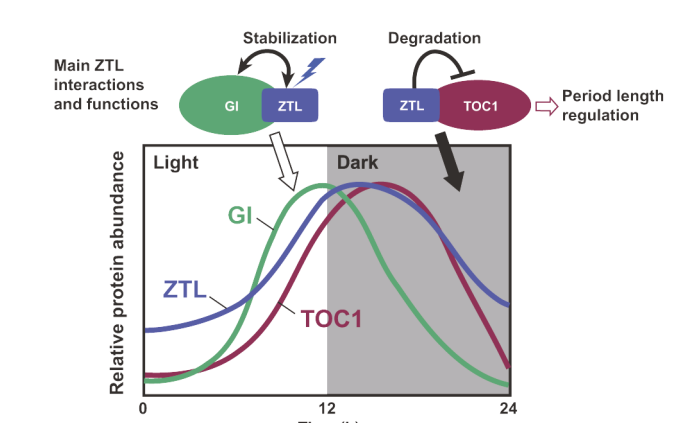


Figure 1—figure supplement 2. Schematic diagram of the daily protein abundance profile of ZTL and its function in the circadian clock. ZTL function in the circadian clock involves interactions with two core clock proteins, GI and TOC1. The protein abundance patterns of ZTL, GI, and TOC1 proteins are based on previously published results (19, 25). The circadian clock

regulates the expression profile of GI protein with its peak near the end of the light period. The ZTL-GI interaction is enhanced when the ZTL LOV domain absorbs blue light. This interaction stabilizes both ZTL and GI proteins toward the end of the day, thus ZTL protein level also peaks at that time, although ZTL transcript levels are constitutive. TOC1 expression is also clock regulated with expression mainly during the nighttime. ZTL interacts with TOC1 in a light-independent manner, however ZTL mediated TOC1 degradation is enhanced at night. ZTL mutants lead to enhanced accumulation of TOC1 protein, leading to period lengthening of the circadian clock.

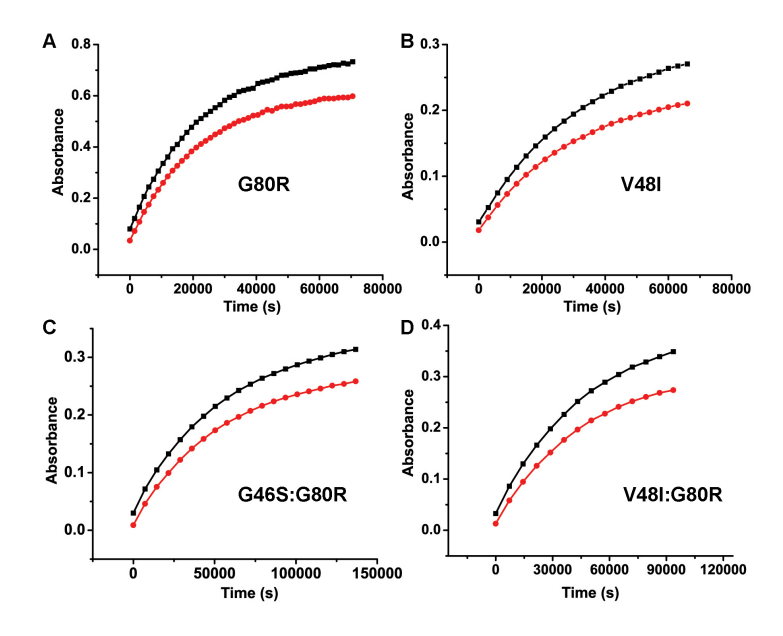


Figure 1—figure supplement 3: Kinetics of ZTL Variants (A-D) Kinetics of ZTL adduct decay are determined from the absorbance recovery at 450 (black) and 478 nm (red). G80R; τ =6.6 hr (A) and V48I; τ =10.7 hr (B) recover on similar timescales. The G46S:G80R; τ =21 hr (C) variant recovers with a 2-fold slower time constant. A V48I:G80R variant recovers τ >65 hours (see Table 1 for more information). Due to the long time constant for V48I:G80R, full recovery cannot be observed without the presence of an imidazole base catalyst (13). The recovery data shown (D) is under base catalyzed conditions (150 mM imidazole) to allow full recovery.

1130

1131

1132

1133

1134

1135

1136

1137

1138

1139

1140

1141

1142

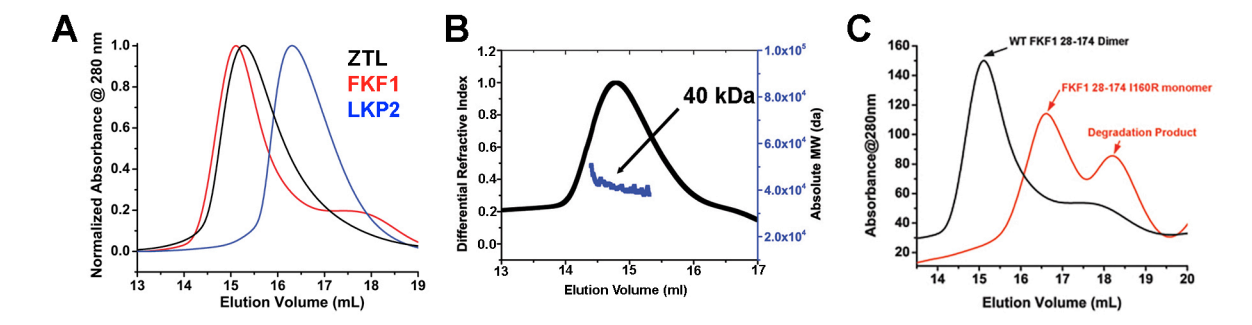


Figure 2—figure supplement 1: Dimerization of ZTL/FKF1/LKP2 LOV domains. (A) ZTL (16-165; apparent MW=57 kDa; absolute MW from MALS ~40 kDa, panel B) and FKF1 (28-174;

confirmed by multi-angle light scattering (B). LKP2 (16-165 apparent MW=33 kDa) adopts a

apparent MW from SEC 62 kDa; absolute MW from MALS ~42 kDa) elute as dimers on SEC as

much smaller hydrodynamic radius indicating distinct differences in oligomeric structure and/or

affinity. ZTL 16-165 was used to allow comparison of similar length constructs and allow use of

a stable FKF1 construct characterized previously (39), B) Multi-angle light scattering of ZTL 16-165. The expected monomer MW was ~18 kDa, indicating ZTL exists as a constitutive dimer.

(C) Introduction of I160R variants (equivalent to ZTL I151R) in FKF1 renders the protein

monomeric. It is also more susceptible to proteolysis.

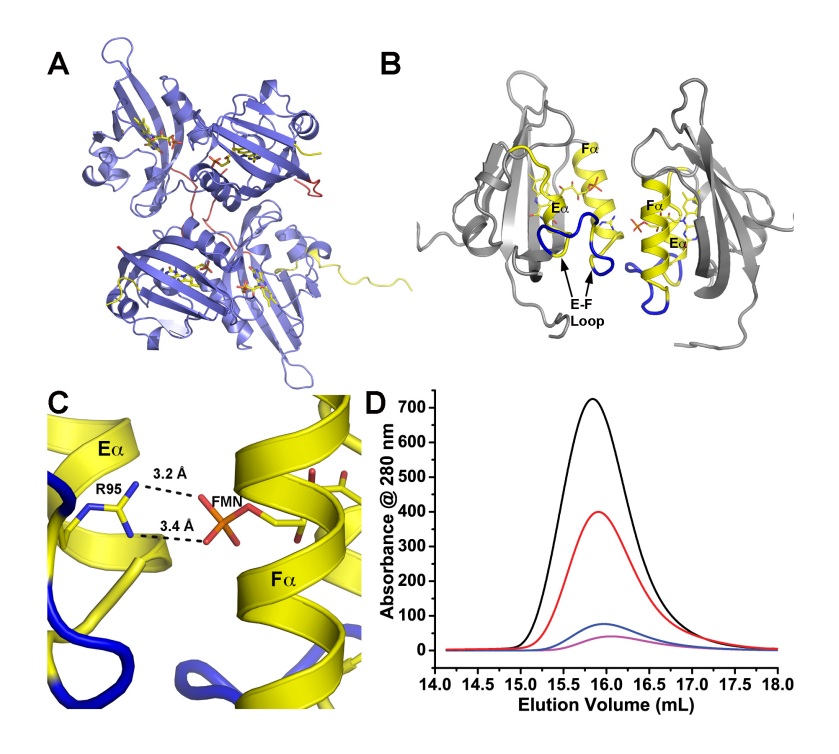


Figure 2—figure supplement 2. Dark-state structure of ZTL 29-165 and helical dimer. (A) ZTL crystallizes as a tetramer, where the helical interfaces are buried within the crystal lattice. (B) A parallel helical dimer is observed in the crystal lattice that is characterized by slightly asymmetric contacts between the E and F helices (yellow) and associated loops (blue). (C) Contacts between R95 in the E-F loop (blue) and the phosphate of the bound FMN of the neighboring molecule stabilize the helical dimer. (C) Introduction of a R95A variant does not affect *in vitro* dimerization of ZTL 29-165. The elution profile of R95A is not concentration dependent and reflects a dissociation constant unable to be determined by SEC (K_d <0.2 μM). Traces depicted and apparent MWs are: dark-state (Black- 41.3 kDa at 130 μM and Blue- 39.6 kDa at 13 μM), light-state (Red-40.8 kDa at 130 μM and Magenta- 37.8 at 13 μM).

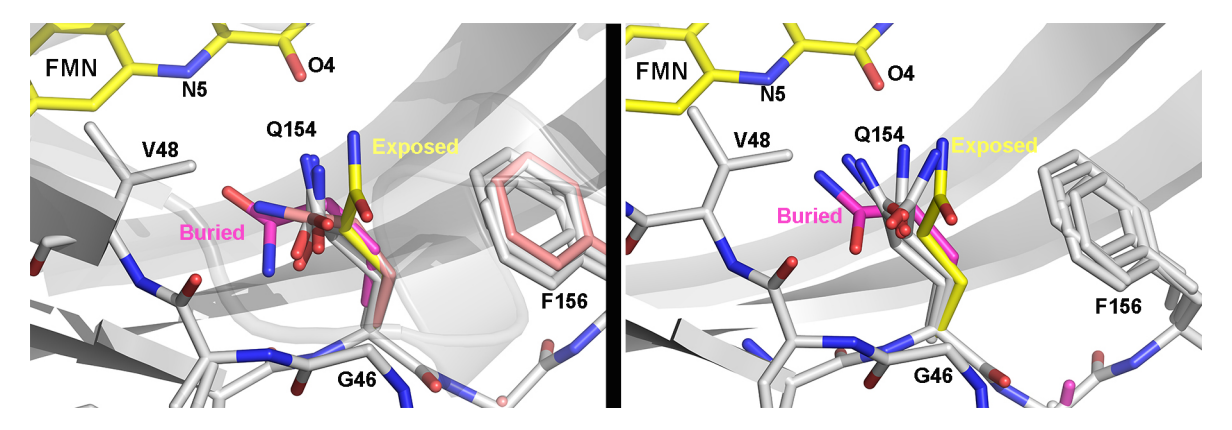


Figure 3—figure supplement 1. Heterogeneous orientations of Q154. WT (left) and G80R (right) conformations of Q154 compared to buried conformations in VVD (magenta; PDBID 2PD7) and exposed conformations in ZTL V48I:G80R (yellow). In both WT and G80R, Q154 samples orientations covering the range between exposed and buried conformations. One orientation in WT (salmon) lies close to the buried conformation. These heterogeneous conformations may contribute to ZTL retaining light and dark-state functions.

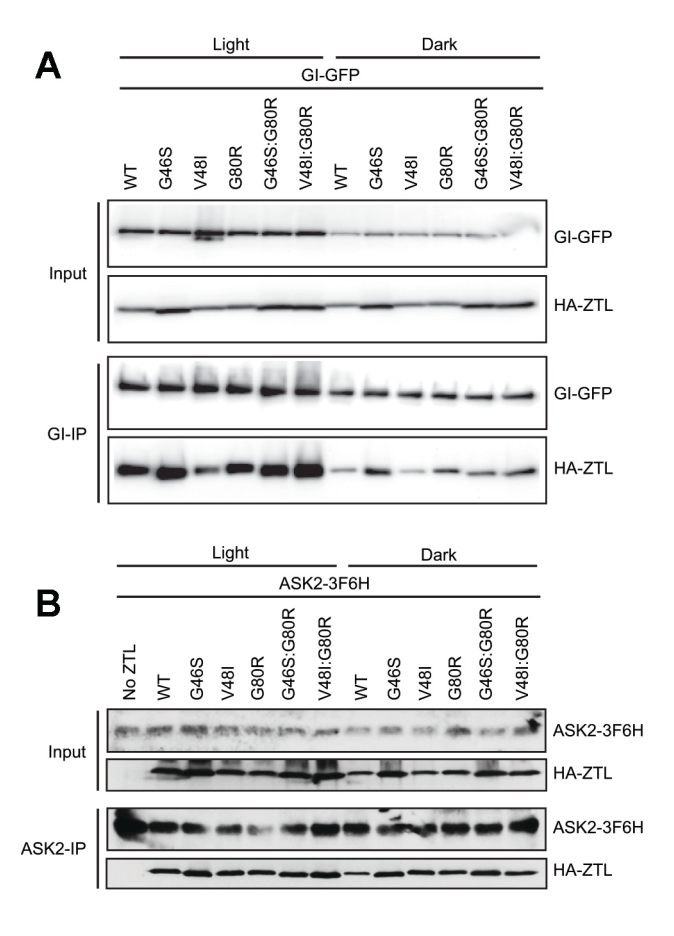


Figure 4—figure supplement 1. Effect of ZTL variants on protein complex formation. (A) *In vivo* interactions between GI and ZTL variants were detected by transient co-expression in *N. benthamiana* under continuous light or dark conditions. WT and ZTL variants all show enhanced interactions with GI in the presence of light. Ncap variants lead to altered GI interactions. V48I disrupts light-state GI interactions, consistent with altered conformational changes. G46S enhances dark-state binding to GI due to partial dark-state activation. These identify the Ncap as the interaction surface for GI. (B) Effect of ZTL LOV domain mutations on ASK2. Proteins were precipitated with anti-FLAG (B) or protein A antibody, and the presence of ZTL variants was detected by anti-HA antibody. All variants indicate that ASK2 interacts with ZTL regardless of lighting conditions.

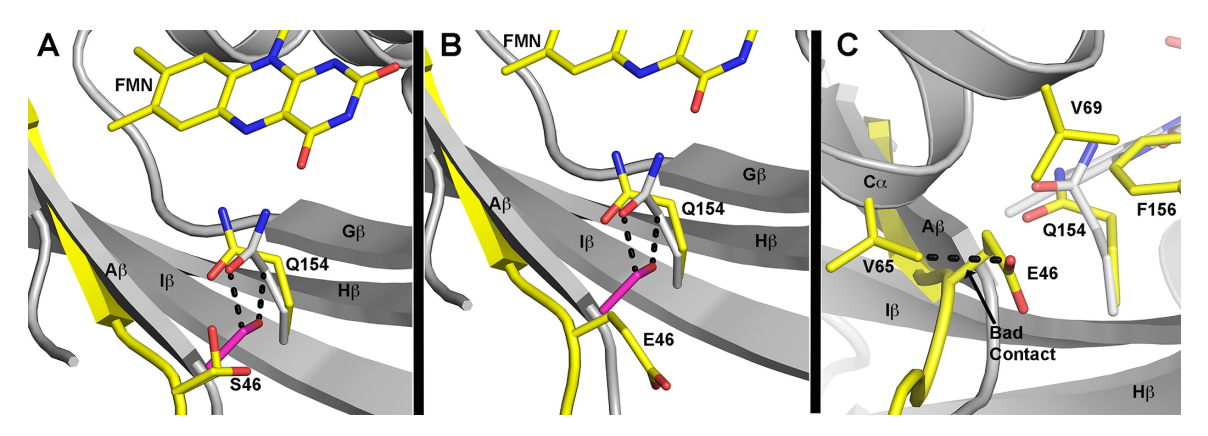


Figure 4—figure supplement 2: Predicted differences in G46 mutants. (A-C) Predicted models of G46 mutations and hypothetical effect based on WT ZTL structures. (A) The WT ZTL (grey cartoon) structure cannot accommodate a sidechain at position 46. Addition of a Ser residue (G46S) at this position leads to steric clashes (2.2 Å) between the Cβ position and the exposed conformation (grey) of Q154. Additional clashes are present from the OH group (dashed lines). G46S can be accommodated by very modest movement of Aβ (yellow) and rotation of Q154 to the buried position (yellow). Such reorientation favors the putative light-state conformation of Q154. S46 can adopt to orientations that do not clash with any residues in the

ZTL structure (shown). One orientation H-bonds with Q154. Such interactions should not disrupt the ZTL fold. (B) The equivalent orientation of the Glu sidechain in a G46E that minimizes steric clashes. (C) A G46E mutation requires rotation of the Glu sidechain out of the active site pocket. The orientation with minimum steric clashes retains a van der Waals contact (2.5 Å) with V65 in $C\alpha$ (dashed line). In addition, charged E46 is forced into a hydrophobic pocked lined by V65, V69 and F156. We predict these combined interactions destabilize the LOV fold in G46E.

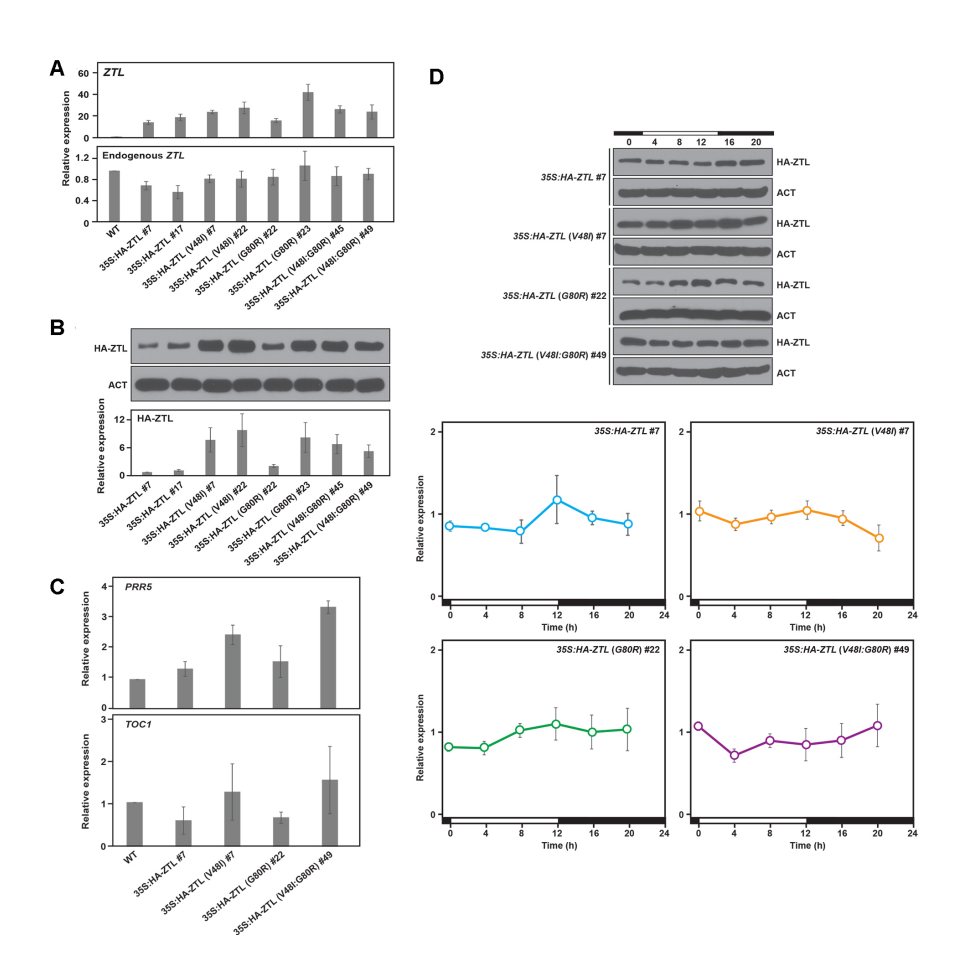


Figure 5—figure supplement 1: Relative expression levels of clock proteins. Expression levels of total *ZTL* and endogenous *ZTL* transcripts (A), and also *ZTL* protein (B) were analyzed in WT, 35S: HA-ZTL, 35S: HA-ZTL (V48I), 35S: HA-ZTL (G80R) and 35S: HA-ZTL (V48I:G80R) plants harvested at ZT8 under 12L/12D conditions. (A) Relative expression levels of *ZTL* were

determined using *IPP2* as the internal control. (B) Representative blot images of HA-ZTL and ACT are shown. Relative expression levels of ZTL protein were determined from three biological replicates. C) Expression levels of *PRR5* and *TOC1* transcripts were analyzed in WT, 35S: HA-ZTL, 35S: HA-ZTL (V48I), 35S: HA-ZTL (G80R) and 35S: HA-ZTL (V48I:G80R) plants harvested at ZT8 under 12L/12D conditions. Relative expression levels of *PRR5* and *TOC1* were determined using *IPP2* as the internal control. D) Diurnal expression levels of ZTL protein were analyzed in 35S: HA-ZTL, 35S: HA-ZTL (V48I), 35S: HA-ZTL (G80R) and 35S: HA-ZTL (V48I:G80R) plants under 12L/12D conditions. Representative blot images of HA-ZTL and ACT are shown. Relative expression levels of ZTL protein were determined using ACT as the internal control. All data represent averages ±SEM obtained from three biological replicates

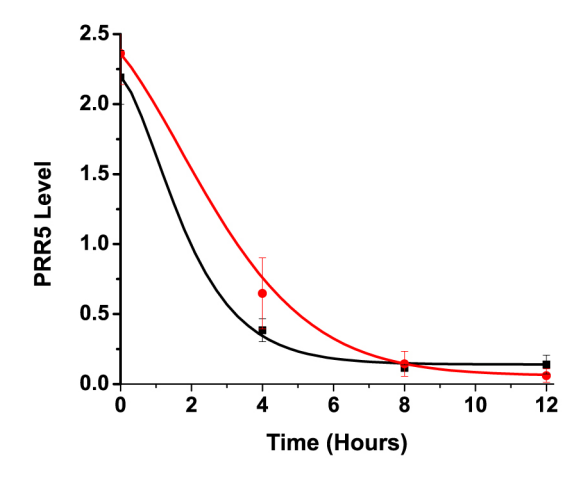


Figure 5—figure supplement 2: Comparison of model to PRR5 degradation in vivo. Comparison of PRR5 degradation model (Eq. 1 and Eq. S10) with experimental data. The red curve (simulated for G80R) shows reasonable precision in predicting the observed delay in PRR5 degradation for G80R data (red circles) compared to simulated WT (black) and WT data (black squares). See methods for model generation and parameter estimation.

```
AtZTI.
             44 PCGFVVTDAVEPDOPTTYVNTVFEMVTGYRAEEVT.GGNCRFT.OCRGPFAKRRHPT.VDS 101
AtLKP2
             40 PCGFVVSDALEPDNPIIYVNTVFEIVTGYRAEEVIGRNCRFLOCRGPFTKRRHPMVDS 91
             44 PCGFVVTDALDPDHPIIYVNTVFEIVTGYCAEDVLGRNCRFLOCRGPFAKRRHPLVDS 101
GmZTL
OsZTL1
             57 PCGLVVTDALEPDCPIIYVNCGFEEATGYRAEEVLGRNCRFLOCRGPFAORRHPLVDA 114
             53 ACGLVVSDALEPDFPIIYVNRGFEDATGYRAEEVLGRNCRFLQCRGPFAKRRHPLVDT 110
OsZTL2
             38 PCGFVVTDSLEPDHPIIYVNTVFEMVTGYRAEEVLGRNCRFLQCRGPFAKRRHPLVDS 95
CsZTL
             45 PCGFVVTDALEPDHPIIYVNSVFESITGYRAEDVLGRNCRFLQCRGPFAKRRHPLVDS 102
CcZTL
GhZTL
             37 PCGFVVTDALESDHPIIYVNTVFEMVTGYRAEEVLGRNCRFLOCRGPFAKRRHPLVDS 94
ZmZTL1
             56 PCGLVVTDALEPDCPIIYVNRGFEEATGYRAEEVLGRNCRFLQCRGPFARRHPLVDA 113
ZmZTL2
             39 ACCMVVSDALEPDFPIIYVNRGFESSTGYSAEEVLGRNCRFLQCRGPFAQRRHPLVDA 96
             46 ACGLVVSDALEPDFPIIYVNRGFEDATGYHAEEVLGRNCRFLQCRGPFAQRRHPLVDA 103
BdZTL1
             87 PYGLVVTDALEPDCPIIYVNRGFEEATGYRAEEVLGRNCRFLQCRGPFAQRRHPLVDA 145
             58 PCGLVVTDALEPDCPIIYVNRGFEDATGYRAEEVLGRNCRFLQCRGPFAQRRHPLVDA 115
SiZTL1
             46 ACGMVVSDALEPDFPIIYVNRGFEDATGYRAEEVLGRNCRFLQCRGPFAQRRHPLVDT 103
SiZTL2
             37 TFGFVVTDALDPDHPIIYVNTVFEIITGYRADEVIGKNCRFLQCRGPYAKRRHPSVDS 94
Bra038832
             40 PCGFVVSDALEPDQPIIYVNAVFEIVTGYRAEEVIGRNCRFLQCRGPYAKRRHPSVDS 97
Bra038831
Bra038830
             40 PCGFVVSDALEPDQPIIYVNTVFEIVTGYRAEEVIGRNCRFLQCRGPYAKRRHPSVDS 97
MpFKF1
             60 PCGLIVTDALEPDOPIIYVNTVFEFITGYKAEEILGKNCRFLOCRGPFAORRHPLVDP 117
SmFKF1
              4 PCSVVVTDALDVDFPIIYVNNIFEFITGYKAEEVLGRNCRFLQFRGPFAQRRHPLVDS 61
AtFKF1
             52 PPSFIVSDALEPDFPLIYVNRVFEVFTGYRADEVLGRNCRFLQYRDPRAQRRHPLVDP 109
GmFKF1
             48 PTSFVVSDALEPDFPIIYVNKVFEISTGYRADEALGRNCRFLQYRDPRAQRRHPLVDP 105
OsFKF1
             64 AAAIVVSDAVEVDFPVIYVNAAFEAATGYRADEVLGRNCRFLQFRDPRAQRRHPLVDP 121
             57 PTSFVVSDALEPDFPIIYVNKVFEIFTGYRADEVLGQNCRFLQYRDPRAQRRHPLVDP 114
CsFKF1
             72 PTSFVVADAFDPDFPIIYVNKVFEIFTGYRADEVLGRNCRFLQYRDPRAQRRHPLVDP 129
CcFKF1
GhFKF1
             55 PTSFVVSDALEPDFPVIYVNKVFEVFTGYRADEVLGRNCRFLQYRDRRAQRRHPLVDP 112
ZmFKF1
             42 PAAILVADAAEVDFPVIYVNAAFEAATGYRAHEVLGRNCRFLQFRDPHAQRRHPLVDP 99
BdFKF1
             57 AAAIVVADAVEPDFPVIYVNAAFEAATGYRAHEVLGRNCRFLQFRDPRAQRRHPLVDP 114
SiFKF1
             AtLOV2
            477 EKNFVITDPRLPDNPIIFASDSFLELTEYSREEILGRNCRFLOG-----PETDL 522
GmT-OV2
            457 EKNFVITDPRLPDNPIIFASDSFLELTEYSREEILGRNCRFLOG-----PETDP 505
OsLOV2
            412 EKNFVITDPRLPDNPIIFASDSFLQLTEYNREEILGRNCRFLQG-----PETDR 460
ZmLOV2
            400 EKNFVITDPRLPDNPIIFASDSFLRLTEYCREEILGRNCRFLQG-----PETDR 448
BdLOV2
            409 EKNFVITDPRLPDNPIIFASDSFLQLTEYCREEILGRNCRFLQG-----PETDR 457
            412 EKNFVITDPRLPDNPIIFASDSFLQLTEYSREEILGRNCRFLQG-----PETDR 460
AsLOV2
                                         * * .: :* ***** E-F Loop * .*
                            * *:*:.. *
AtZTI.
            102 MVVSEIRKCIDEGIEFQGELLNFRKDGSPLMNRLRLTPIYGDDDTITHIIGIQFFIETD 160
AtLKP2
             92 TIVAKMRQCLENGIEFQGELLNFRKDGSPLMNKLRLVPIREEDE-ITHFIGVLLFTDAK 149
GmZTL
            102 TVVSEIRRCLEEGIEFOGELLNFRKDGSPLMNRLRLTPIYGDDETITHVIGIOFFTEAN 160
OsZTL1
            115 MVVSEIRKCIDNGTEFRGDLLNFRKDGSPLMNKLHLTPIYGDDETITHYMGIOFFTNAN 173
OsZTL2
            111 TVVTDIRRCLEEGTVFOGDLLNFRKDGSPFMAKLOLTPIYGDDETITHYMGMOFFNDSN 169
             96 SVVSEIRRCLEDGTEFQGELLNFRKDGTPLMNKLRLTPIYGDDETVTHVIGIQFFTEAD 155
CsZTL
            103 SVVSEIRRCLEEGIEFQGELLNFRKDGSPLMNRLRLSPIYGDDETITHVIGIOFFTEAN 161
CcZTL1
             95 TVVSEIRRCLDEGIEFOGELLNFRKDGSPLMNRLRLTPIYGDDETITHVIGIOFFTEAN 153
GhZTL1
ZmZTL1
            114 ALVSEIRCIDNGIEFRGDLLNFRKDGSPVMNRLHLTPIYGDDETITHYMGIQFFTDAN 172
ZmZTL2
             97 AVVTRIRRCLDEGTEFHGDLLNFRKDCSPYMARLQLTPIYGDDEVITHYMGIQFFNDSN 155
BdZTL2
            104 IVVAEIQRCLEEGTEFQGDLLNFRKDGSPFMTNLQLKPIYGDDETITHYMGIQFFNDSN 162
BdZTL2
            146 AVVSGIQRCIDNGTQFRGDLLNFRKDGFPLMNRLHLTPIYGDDDIITHYMGIQFFTNAN 203
            116 AMVSNIRRCIDNGTEFRGDLLNFRKDGSPLMNRLHLTPIYGDDATITHYMGIQFFTNAN 174
SiZTL1
SiZTL2
            104 AVVSGIRRCLEEGTEFQGDLLNFRKDGSPYMAKLQITPIYGDDDMITHYMGIQFFNDSN 162
Bra038832
             95 TVVSKMRRCLEKGIEFQGELLNFRKDGSPLMNKLRLVPIREDDE-ITHIIGVLFFTDAK 152
Bra038831
             98 TVVSKMRQCLEKGIEFQGELLNFRKDGSPLMNKLRLVPIREEDE-ITHFIGVLSFTDAE 155
Bra038830
             98 TVVSKMRQCLEKGIEFQGELLNFRKDGSPLMNKLRLVPIREDDE-ITHFIGVLSFTDAD 155
MpFKF1
            118 TIVATIKRCLSEGVEFRGELLNFRKDGTPLMNKLCMTPIHAEDGTITHVIGIQSFTEAK 176
             62 ATVTEIRCMREGIEFWGELLNFRKDGTPLMNKLCLKPIRGEDGRITHIIGIOSFSEVK 120
            110 VVVSEIRRCLEEGIEFQGELLNFRKDGTPLVNRLRLAPIRDDDGTITHVIGIQVFSETT
AtFKF1
            106 VVVSEIRRCLEEGVEFQGELLNFRKDGTPLVNRLRLAPIHDDDGTVTHVIGIQLFSEAN 164
GmFKF1
OsFKF1
            122 MVVSEIRRCLNEGIEFQGELLNFRKDGAPLYNRLRLIPMHGDDGFVTHVIGIQLFSEAN 180
            115 VVVSEIRRCLEEGVEFQGELLNFRKDGTPMVNRLRLAPIHDDDGTVTHIIGIQVFSETK 173
            130 VVVSEIRRCLEEGIEFQGELLNFKKDGTPLVNRLRLAPIRDDDGTVTHIIGIQIFSEAK 188
CcFKF1
            113 FVVSEIRRCLEEGIEFEGELLNFRKDGTPLVNRLKLAPIRDDDGIVTHVIGIQVYSEAK 171
GhFKF1
ZmFKF1
            100 MVVSEIRRCLSEGIEFQGELLNFRKDGAPLHNRLRLVPMHGDDGYVTHVIGIQLFSEAN 158
            115 MVVSEMRRCLNDGIEFEGELLNFRKDGAPLNNRLRLIPMHGDDGSMTHIIAIQLFSDAN 173
SiFKF1
            117 MVVSEIRRCLNEGIEFQGELLNFRKDGAPLYNRLRLIPMHGDDGSVTHVIGIQLFSEAN
AtLOV2
            523\ \ TTVKKIRNAIDNQTEVTVQLINYTKSGKKFWNIFHLQPMRDQKGEVQYFIGV\\ \textbf{Q}L\textbf{D}GSKH \ 581
GmLOV2
            506 \ \text{ATVRKIREAIDNQTDVTVQLINYTKSGKKFWNLFHLQPMRDQKGEVQYFIGV} \textbf{QLD} \textbf{GSQH} \ 564
OsLOV2
            461 ATVRKIRDAIDNQAEVTVQLINYTKSGKKFWNLFHLQPMRDQKGDVQYFIGVQLDGTEH 519
ZmLOV2
            449 GTVKKIRDAIDNQTEVTVQLINYTKSGKKFWNLFHLQPMRDQKGDVQYFIGVQLDGTER 507
BdLOV2
            458\ \texttt{ATVRKIRDAIDNQTDVTVQLINYTKSGKKFWNLFHLQPMRDQKGDVQYFIGV} \textbf{QLD} \textbf{GTEH}\ 516
            \tt 461\ ATVRKIRDAIDNQTEVTVQLINYTKSGKKFWNLFHLQPMRDQKGDVQYFIGV\textbf{Q}L\textbf{D}GTEH\ 519
AsLOV2
                  * :: .: . :*:*: *.*
                                                 : : *: :. : : :.:
```

1213

1214

1215

1216

Figure 7—figure supplement 1: Sequence Alignment of FKF1/ZTL family members in plants. ZTL/FKF1/LKP2 homologs from dicots; (*Arabidopsis thaliana* (At), *Brassica rapa* (Bra), *Glycine max* (Gm), *Cucumis sativus* (Cs), *Citrus clementine* (Cc), *Gossypium hirsutum* (Gh),

Avena sativa (As), monocots; Oryza sativa japonica (Os), Setaria italica (Si), Zea mays (Zm),
Brachypodium distachyon (Bd), Liverwort; Marchantia polymorpha (Mp) and Spikemoss;
Selaginella moellendorffii (Sm). ZTL and FKF1 cluster in reference to conserved CGF and QFF
motifs. See Figure S9 for corresponding accession numbers. All ZTL proteins conserve G46
and V48 (blue). In FKF1 the position corresponding to G46 contain Ala (FKF1-like monocots) or
Ser (FKF1-like dicots) (red); Phototropins contain an Asn at the equivalent position (green). *
denote conserved residues through all proteins. All proteins conserve the canonical
GXNCRFLQ motif (magenta) as well as residues leading into the E-F loop. The FKF1 species
differ in the residues immediately following the LOV consensus sequence in the beginning of the
E-F loop (ZTL: C87 and G89; FKF1: F87 and D89). Liverwort and spikemoss sequences
diverge containing elements consistent with both ZTL and FKF1 (G46 and ZTL E-F loop but I48
for Mp; S46 and F87 but G89 for Sm), indicating an evolutionary transition. The QFF (blue) motif
is more divergent. All ZTL/FKF1 contain a Phe at position 156 that occupies an alternative
buried position compared to solvent exposed hydrophilic residues in other LOV proteins.

Table 1:

Kinetics of thermal reversion for LOV constructs and variants at 296 K. Uncertainty is depicted as the standard deviation from 3 replicates.

	<u> 1247</u>
Construct	Time Constant, k₃ [l½ṛ]8
WT ZTL 29-165	1.4 +/- 0.1 1249
G80R	6.6 +/- 0.1 1250
V48I	10.7 +/- 0.81251
G46S:G80R	21 +/- 3 1252
V48I:G80R	65 hrs<τ 1252
	1233

Table S2:

Data collection and refinement statistics (molecular replacement)

	WT ZTL	G80R	ZTL-Dark	ZTL-Light
	Dark	Dark	V48I:G80R	V48I:G80R
PDB ID	5SVG	5SVU	5SVV	5SVW
Data collection				
Space group	P3(1)21	P3(1)21	P3(1)21	P3(1)21
Cell dimensions				
a, b, c (Å)	85.0, 85.0,	85.4, 85.4,	85.4, 85.4,	86.2, 86.2,
	199.5	200.0	198.8	200.5
a, b, g (°)	90, 90, 120	90, 90, 120	90, 90, 120	90, 90, 120
Resolution (Å) *	2.5 (2.59-2.5)	2.6 (2.69-2.6)	2.10 (2.18-2.1)	2.29 (2.35- 2.29)
R_{sym} or R_{merge}	7.6 (27.9)	12.8 (23.4)	5.6 (25.1)	6.1 (19.9)
I/sI	35.0 (11.1)	55.4 (22.7)	36.6 (12.6)	19.8 (5.5)
Completeness (%)	97.1 (98.6)	97.9 (99.8)	99.3 (99.0)	87.0 (84.3)
Redundancy	9.0	10.0	7.9	2.6
Refinement				
Resolution (Å)	2.5	2.6	2.1	2.3
No. reflections	28790	26153	49510	34582
R _{work} / R _{free}	17.8/24.0	16.4/23.2	16.3/20.0	16.2/22.8
No. atoms				
Protein	3964	3990	3986	3950
Ligand/ion	124	124	148	124
Water	142	139	343	269
B-factors				
Protein	47.3	46.8	34.6	37.5
Ligand/ion	35.2	35.4	27.6	27.5
Water	46.8	42.4	41.6	39.6
R.m.s. deviations				
Bond lengths (Å)	0.014	0.014	0.012	0.014
Bond angles (°)	1.58	1.61	1.46	1.65
Ramachandran	2 (0.4%)	3 (0.62%)	1 (0.21%)	1 (0.21%)
outliers				
*Highest_resolution s	hall is shown in	narentheses		

^{*}Highest-resolution shell is shown in parentheses.

Table 3:

Period length estimates of CCA1:LUC activity in WT and ZTL variants overexpression plants.

See Figure 5—figure supplement 1 for expression levels.

Genotype	Estimated Period	HA-ZTL	*Estimated k _{deg}	*Estimated k _{deg}
	length (hrs)	protein	PRR5 LD (hrs 1)	PRR5 LL (hrs -1)
		abundance		
WT	24.36±0.40	ND	0.3 ±0.1	0.13 ±0.1
35S:HA-ZTL #7	23.69±1.23	1	0.5 ±0.1	0.13 ±0.1
35S:HA-ZTL #17	23.65±0.72	1.5 ± 0.3	ND	ND
35S:HA-ZTL (V48I) #7	ND	11 ± 4	0.8 ±0.1	0.5 ±0.2
35S:HA-ZTL (V48I) #22	ND	14 ± 5	ND	ND
35S:HA-ZTL (G80R) #22	24.17±1.08	3 ± 0.5	0.34 ±0.05	0.14 ±0.1
35S:HA-ZTL (G80R) #23	19.33±1.06	12 ± 5	ND	ND
35S:HA-ZTL (V48I:G80R) #45	ND	10 ± 3	0.8 ±0.2	0.3 ±0.2
35S:HA-ZTL (V48I:G80R) #49	ND	7.6 ± 2	ND	ND

 *Estimated k_{deg} values were extracted by fitting Eq. S10 (below) to the PRR5 protein levels *in vivo*. For LD conditions, an average k is obtained by treating the system as only containing dark-state protein. Thus, the LD values are accurate as comparative terms between variants only.